# MÖSSBAUER EFFECT INVESTIGATIONS OF THE HYPERFINE INTERACTIONS AND RELAXATION PHENOMENA IN SALTS OF THULIUM

Thesis by

Milton J. Clauser

In Partial Fulfillment of the Requirements

For the Degree of

Doctor of Philosophy

California Institute of Technology

Pasadena, California

1966

(Submitted March 29, 1966)

## ACKNOWLEDGMENTS

The author would like to express his thanks to Dr. Rudolf Mössbauer for much advice, discussion, and assistance with this work.

The author would also like to express his thanks to Dr. Egbert Kankeleit for his advice and frequent assistance with the experimental work.

Others have contributed to the success of this work. The author would like to thank: Dr. Felix Boehm for creating an atmosphere conducive to productive scientific work. Dr. Frank Snively for his advice on the low temperature experiments. Mr. H.E. Henrikson for his help with the design of various pieces of apparatus. Mr. Vaughn Stephenson and Mr. Ellsworth "Woody" Kiersey for their help in making parts of the apparatus.

The author would also like to thank his wife Patty for her cooperation and forbearance.

This work was supported in part by the National Science Foundation, the United States Atomic Energy Commission, and the Shell Oil Company.

## ABSTRACT

Two new phenomena have been observed in Mössbauer spectra: a temperature-dependent shift of the center of gravity of the spectrum, and an asymmetric broadening of the spectrum peaks. Both phenomena were observed in thulium salts. In the temperature range $1^{o}K \leq T \leq 5^{o}K$ the observed shift has an approximate inverse temperature dependence. We explain this on the basis of a Van Vleck type of interaction between the magnetic moment of two nearly degenerate electronic levels and the magnetic moment of the nucleus. From the size of the shift we are able to deduce an "effective magnetic field" $H = (6.0 \pm 0.1) \times 10^{6}$ Gauss, which is proportional to $\langle r^{-3} \rangle_{M} \langle G | \vec{J} | E \rangle$ where $\langle r^{-3} \rangle_{M}$ is an effective magnetic radial integral for the 4f electrons, and $|G\rangle$ and $|E\rangle$ are the lowest 4f electronic states in $Tm\ Cl_3 \cdot 6H_2O$. From the temperature dependence of the shift we have derived a preliminary value of 1 $cm^{-1}$ for the splitting of these two states. The observed asymmetric line broadening is independent of temperature in the range $1^{o}K \leq T \leq 5^{o}K$, but is dependent on the concentration of thulium ions in the crystal. We explain this broadening on the basis of spin-spin interactions between thulium ions. From the size and concentration dependence of the broadening we are able to deduce a spin-spin relaxation time for $Tm\ Cl_3 \cdot 6H_2O$ of the order of $10^{-11}$ sec.

# TABLE OF CONTENTS

# INTRODUCTION

Two new phenomena have been observed in Mössbauer spectra: a new, temperature-dependent shift of the center of gravity of the spectra, and an asymmetry of the line shape due to spin-spin interactions. Both of these phenomena have been observed in salts of thulium, but are expected to occur in other salts as well.

The shift of the center of gravity reported in this thesis occurs at temperatures in the liquid helium range and below. We explain this shift on the basis of an interaction of the nuclear dipole moment between two nearly degenerate 4f electronic levels, i.e., a Van Vleck type of interaction between the nuclear and electronic moments. Several other types of shifts of the center of gravity of the spectrum have been reported in the literature: 1. the isomer shift[1)], 2. the second order Doppler shift[2)], and 3. shifts due to a reduction of the areas of some of the spectrum lines caused by effects such as an anisotropic Debye-Waller factor (the Karyagin effect)[3)]. The shift which we observe does not have the temperature dependence to be expected from 1. and 2., and the areas of our observed spectrum lines are not reduced, eliminating 3. as a possible cause of the shift we observe.

The second phenomenon reported in this thesis is an asymmetry of the line widths, which at low temperatures is independent of temperature, but varies as a function of the concentration of thulium ions in the crystal. The importance of the phenomenon is that information can now be extracted not only from the positions of the

gamma lines, determined by the hyperfine interactions, but also from the line shapes, affected by interactions of the central ion with its surroundings (e.g., spin-spin and spin-lattice interactions). The scope of Mössbauer spectroscopy is thereby advanced to cover an area of study similar to that covered by NMR and EPR spectroscopy, where information is deduced both from the shapes and the positions of the lines.

We have studied spectra of three salts which show one or both of these phenomena: Tm $Cl_3 \cdot 6H_2O$, $Tm_2(SO_4)_3 \cdot 8H_2O$, and Tm O I. Our main emphasis is on the chloride results since information is not presently available on the electronic level structures of the sulphate and the oxy-iodide but is available indirectly on the chloride.

## THEORY

### The Shift of the Center of Gravity of Mössbauer Spectra[4)]

The main requirement for a temperature dependent shift such as we observed is that the electronic levels have a state $|E\rangle$ located at $k\theta$, about 1 $cm^{-1}$ or less, above the ground electronic state $|G\rangle$. In rare earth salts for example, this condition can be satisfied if the lowest levels of the 4f electrons are nearly degenerate, or by applying a magnetic field if the lowest level is degenerate. If we consider the hyperfine interactions of the nucleus with the electrons we now have two parts to take into account. First there is the usual part of the interaction which involves matrix elements like $\langle G, e|H_{hf}|G,e'\rangle$, where e,e' refer to the nuclear substates. Here, e refers to the nuclear excited state and g will refer to the nuclear ground state. These matrix elements are diagonal elements with respect to the electronic states, though they may also contain cross terms, like $\langle G, e|H_{hf}|G',e'\rangle$, between <u>degenerate</u> electronic states. This part of the hyperfine interaction produces the usually-observed hyperfine spectrum (e.g., the quadrupole splitting) with no shift in the center of gravity of the spectrum. This will be referred to as the "diagonal" part of the interaction. The second part (or "off-diagonal" part) of the hyperfine interaction involves off-diagonal terms like $\langle G, e|H_{hf}|E, e'\rangle$ between <u>non</u>-degenerate electronic states. In our case, these are magnetic interactions. As is well known, this type of term causes the energy levels to repel each other so that the states $|G, e\rangle$ are shifted down in energy while the states $|E, e\rangle$ are

Figure 1

Hyperfine Energy Levels and Spectrum Lines in $TmCl_3 \cdot 6H_2O$

1A. The two lowest electronic levels $|E\rangle$ and $|G\rangle$ are shown with and without hyperfine interactions. For the purposes of this drawing it was assumed that the field gradients of the two CEF levels were identical, as this is nearly true for $TmCl_3 \cdot 6H_2O$.

1B. The Mössbauer spectrum which is associated with Figure 1A is shown. The notation $a \rightarrow c$ refers to gamma transitions between levels marked a and c in Figure 1A. The lines are also labeled 1 - 4 for comparison with the transitions in Figure 2. The small line at $E_0$ is the center of gravity of lines 2 and 3.

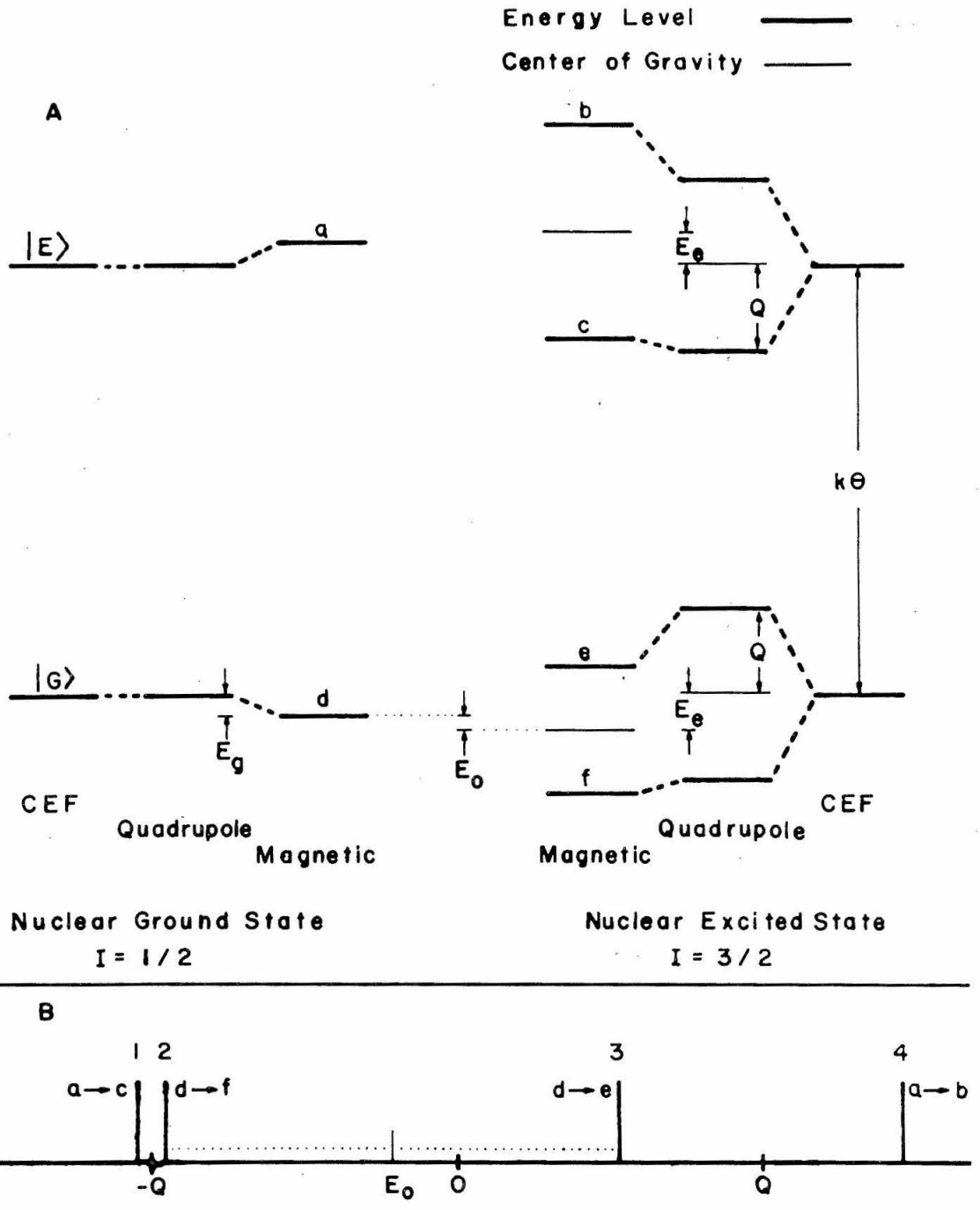


Figure 1.

HYPERFINE ENERGY LEVELS AND SPECTRUM LINES IN $TmCl_3 \cdot 6H_2O$

shifted up (see Figure 1). Now, of course this consideration applies to both the nuclear ground state and the nuclear excited state, though the shifts will generally be different for the nuclear ground state than for the nuclear excited state. It is just this difference which will be observed in a gamma-ray spectrum.

Let us say that the shift of the center of the levels associated with the nuclear ground states and electronic ground state $|G,g\rangle$ is $-E_g$ (for thulium, which is illustrated in Figure 1A, the nuclear ground state is unsplit so that $-E_g$ is just the shift of this level). Similarly, the shift of the center of the levels associated with the nuclear excited states and the electronic ground state, $|G,e\rangle$, is $-E_e$ (for thulium the nuclear excited state is split into two levels, the center of which is halfway in between, as illustrated in Figure 1A). The shift of the center of the spectrum lines associated with the ground electronic level is:

$$E_0 = E_g - E_e . \tag{1}$$

Similarly, the shift of the center of the spectrum lines associated with the excited electronic level is $-E_0$ (see Figures 1B and 2). At high temperatures both electronic levels are equally populated so that both sets of spectrum lines are equally weighted, and no shift is observed. At a temperature T comparable to $\theta$, the intensity of the spectrum lines associated with the excited electronic state is decreased by a factor $e^{-\theta/T}$. It is then easy to show that the center of gravity of the spectrum is shifted by

Figure 2

Transitions in the Presence of Axially Symmetric Hyperfine Interactions. Shown are the principle gamma transitions. As mentioned in the text, there are four other possible gamma transitions, but these are of negligible intensity. Also shown are the electronic relaxation transitions. Any other relaxation transition, which would involve simultaneous nuclear and electronic spin flips are "forbidden".

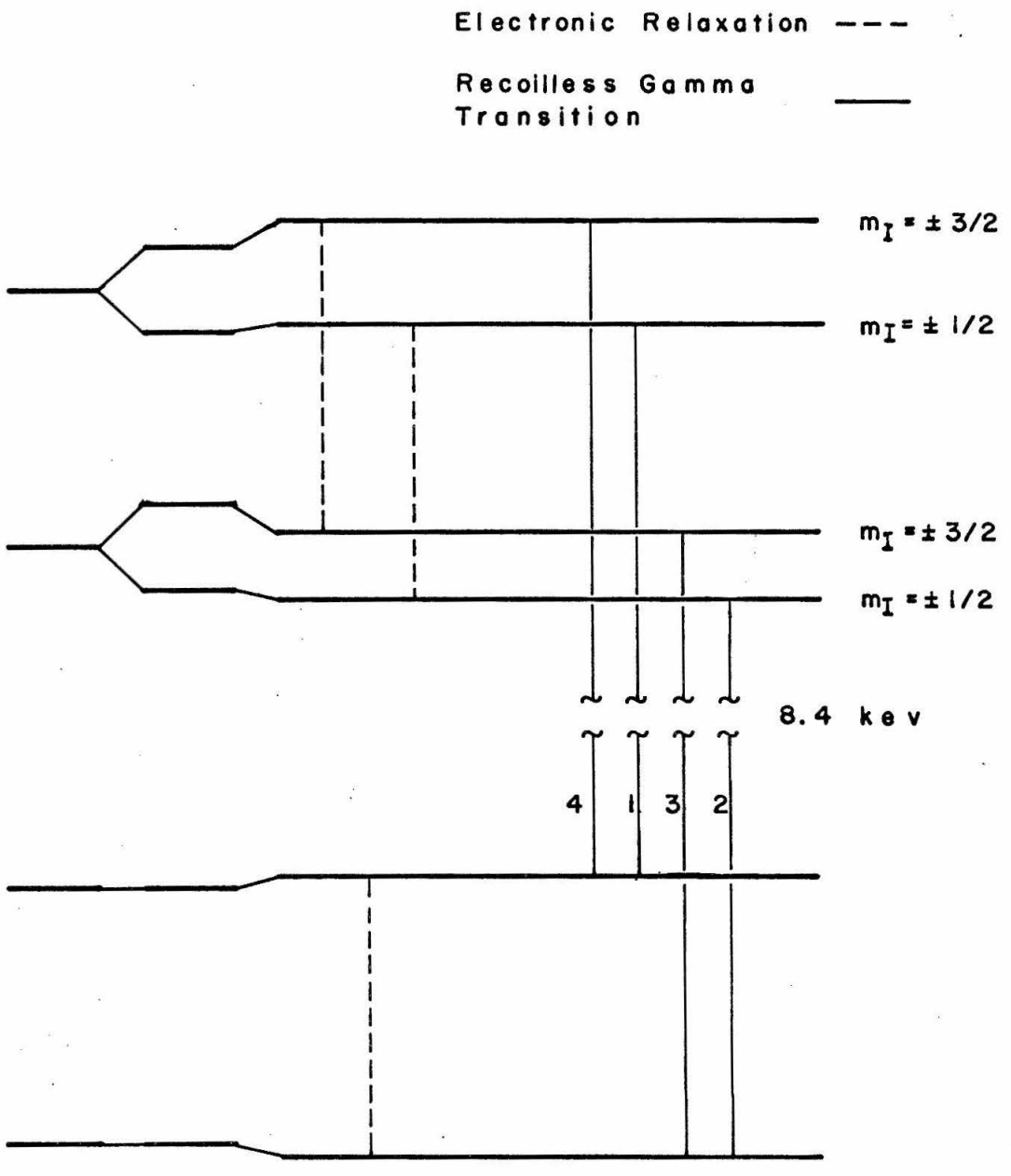


Figure 2

TRANSITIONS IN THE PRESENCE OF AXIALLY SYMMETRIC HYPERFINE INTERACTIONS

$$E_c = E_0 \text{ Tanh } \theta/2T . \qquad (2)$$

It should be emphasized here that the net shift of all the energy levels is zero. It is only the center of gravity of the spectrum that is changing due to temperature dependent Boltzmann factors.

One added result of the "off-diagonal" hyperfine interaction is that it mixes the electronic wave functions so that nuclear transitions accompanied by simultaneous electronic transitions are no longer forbidden. The spectrum lines due to these transitions will be decreased in intensity, and are located at energies of $\pm k\theta$ (+ hyperfine energies) away from the center of the spectrum. Also, $\theta$ may vary, due to distortions, from ion to ion in the crystal, causing the lines to be broadened. Hence, it may be difficult to observe these lines except in the most favorable cases (for example, where $\theta$ is comparable to the hyperfine interactions - about 0.2 $cm^{-1}$ or less in rare earths). These lines have not been observed in thulium.

The 4f Electronic States of Thulium

The trivalent ions of the Lanthanide series of rare earths consist of a xenon core plus a partially filled 4f shell. The 4f shell lies inside the 5s and 5p closed shells. Consequently the 4f electrons are shielded somewhat from interactions with the surrounding ions. This shielding prevents the 4f electrons from playing an appreciable part in chemical interactions, consequently, all the rare earths have quite similar chemical properties. The shielding also has the rather important physical consequence that the interaction of the 4f shell with the Crystalline Electrical Field (CEF) is reduced. Unlike the iron

transition elements, the spin-orbit interaction is stronger than the CEF interaction in the rare-earths. The spin-orbit interaction splits the 4f levels into multiplets for which the total angular momentum, J, is a "good" quantum number. The multiplets (called "J multiplets") are separated by several thousand $cm^{-1}$. These multiplets are split by the CEF into levels which span several hundred $cm^{-1}$. We will be concerned only with the lowest few of these CEF levels.

The lowest J-multiplet of $Tm^{3+}$, which is designated $^3H_6$, with J = 6, has 13 non-degenerate levels in $Tm\,Cl_3 \cdot 6H_2O$ and $Tm_2(SO_4)_3 \cdot 8H_2O$ since the symmetry is only $C_2$ (a two-fold axis of rotation). Unfortunately, little is known about these levels from direct observation. Apparently the lowest two levels are nearly degenerate in both compounds, as Hüfner[5] has studied an optical Zeeman splitting of these levels and has obtained an upper limit for the separation of the levels of about 1 $cm^{-1}$.

In spite of the lack of any other direct information on Thulium, we do have some indirect information. The crystal structure of both $Gd\,Cl_3 \cdot 6H_2O$ [6] and $Eu\,Cl_3 \cdot 6H_2O$ [7] have been worked out. Both of these are typical of an isostructural series which includes all the rare earths from $Pr^{3+}$ to $Lu^{3+}$. The spectra of a number of the rare earth hydrated chlorides has been measured and CEF parameters have been determined from these spectra. A large number of optical transitions in $Er\,Cl_3 \cdot 6H_2O$ have been observed, and from the positions of these lines Harrop[8] has calculated the CEF interaction produced by the surrounding lattice. If it is assumed that the same fields interact

with the Thulium ion, then we can get a fair description of the CEF levels for $Tm\ Cl_3 \cdot 6H_2O$. Harrop has extended this idea to all the rare earths from Gadolinium to Ytterbium. He obtains reasonable agreement with the observed spectra of the Kramer's ions (odd number of electrons - Er, Dy, Yb, Gd) and fair agreement for non-Kramer's ions (Tb, Ho, Tm).

The level scheme calculated for $Tm\ Cl_3 \cdot 6H_2O$ is shown in Figure 3. The principle features of the levels are: there are two sets of nearly degenerate levels, one of which contains the ground state; furthermore, the pair of lowest levels lies about 240 $cm^{-1}$ below the next lowest level so that at low temperatures only the lowest two levels need be considered. The calculated splitting of these two levels is about 0.6 $cm^{-1}$. Using Harrop's crystal field parameters we have calculated the wavefunctions of these two levels (see Appendix I). Using these wavefunctions we have calculated matrix elements for the hyperfine interactions with the $Tm^{169}$ nucleus. We will denote the lowest CEF state by $|G\rangle$ and the first excited state by $|E\rangle$. Since both of these states are non-degenerate and there is presumably, no magnetic field from other ions, symmetry under time-reversal implies that:

$$\langle G|\vec{J}|G\rangle = 0 = \langle E|\vec{J}|E\rangle \ . \qquad (3)$$

There is, however, an off-diagonal matrix element of $\vec{J}$ which does produce a magnetic hyperfine interaction:

$$|\langle G|\vec{J}|E\rangle|^2 = 34.8. \qquad (4)$$

Figure 3

Calculated Crystal Field Levels of $Tm\,Cl_3 \cdot 6H_2O$, $^3H_6$.

These levels were calculated using CEF parameters from Harrop[8] listed in Table II.

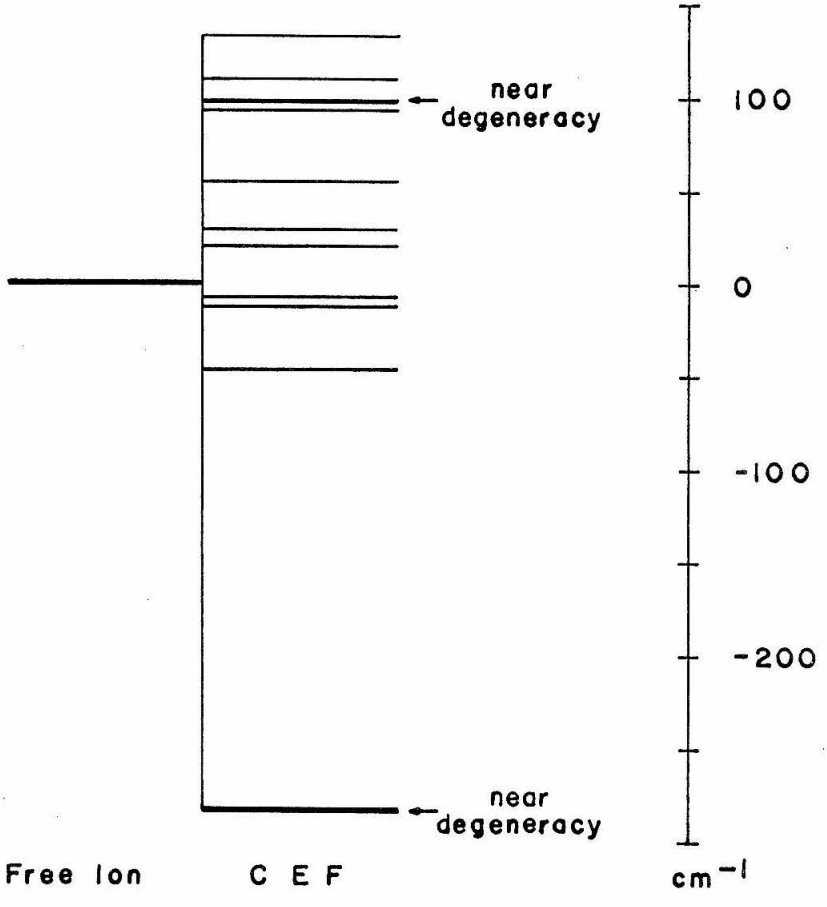


Figure 3

CALCULATED CRYSTAL FIELD LEVELS OF $TmCl_3 \cdot 6H_2O$, $^3H_6$

The matrix elements relevant to the electric field gradient tensor are of the form $1/2 \langle G|J_i J_j + J_j J_i|G\rangle$ where i,j = x,y,z (see Appendix II). In the principal axes coordinate system of this tensor we calculate that:

$$J_z^2 = 2.3 \qquad J_y^2 = 4.6 \qquad J_x^2 = 35.1 \tag{5}$$

for the ground state, and

$$J_z^2 = 2.6 \qquad J_y^2 = 4.2 \qquad J_x^2 = 35.2 \tag{6}$$

for the excited state. We note in particular that the field gradients are nearly identical for the two states. This seems to be a situation peculiar to the ground state in thulium chloride, for in general, in both Kramer's and non-Kramer's salts nearly degenerate levels will not necessarily have similar field gradient tensors. For example, the field gradients of the other nearly degenerate pair of levels in thulium chloride are not nearly so similar.

We should note, however, that the symmetry of the crystal (a 2-fold axis of rotation) requires only that one of the principal axes of each of these tensors (the z axis) coincide with the symmetry axis. As it happens, the x axes of the tensors of the two CEF states and the direction of the vector $\langle G|\vec{J}|E\rangle$ all coincide to within about $1^o$ of arc.

If $J_y^2 = J_z^2$ we would have axial symmetry around the axis of the electric field gradient and the magnetic dipole field. Since this is nearly the case, we will assume axial symmetry of the hyperfine inter-

actions in some of the following discussion in order to get a good qualitative understanding of what is happening. Most of our calculations, however, did not use this assumption.

The surrounding ions in the lattice also contribute to the field gradient tensor, but we have calculated that the main effect is to make the field gradient more nearly axially symmetric, reduce the strength of the field gradient somewhat, and change the direction of the x and y axes slightly.

In our case, the magnetic interaction between nuclear and electronic moments is much stronger than the "off-diagonal" quadrupole interaction. The electronic moment is similar to the Van Vleck magnetic moment, since it comes from a term of the form $\langle G|\vec{J}|E\rangle$. The hyperfine interaction (see Appendix III) is then given by

$$H_M = g\,\beta_N M(\vec{I}\cdot\vec{J}) \tag{7}$$

where $M = 2\beta\,\langle r^{-3}\rangle_M \langle J||N||J\rangle$, g is the nuclear g factor, $\beta$, $\beta_N$ are the Bohr and nuclear magnetons, respectively. We may use perturbation theory to calculate the shifts of the levels under the assumption that the hyperfine interactions are small, compared to $k\theta$. For the detailed derivation, see Appendix IV. The net shift of the spectrum lines is given by

$$E_c = 1/3\,\frac{\beta_N{}^2 M^2\,|\langle G|\vec{J}|E\rangle|^2}{k\theta}\left[g_g{}^2 I_g(I_g+1) - g_g{}^2 I_e(I_e+1)\right]\mathrm{Tanh}\,\frac{\theta}{2T}. \tag{8}$$

If we write the "effective field" as

$$\vec{H} = M\langle G|\vec{J}|E\rangle \tag{9}$$

and the nuclear moment as

$$\mu^2 = g^2 \beta_N{}^2 I(I + 1) \tag{10}$$

we may rewrite (8) as

$$E_c = 1/3 \frac{(\vec{H})^2}{k\theta} (\mu_g{}^2 - \mu_e{}^2) \text{ Tanh } \frac{\theta}{2T} . \tag{11}$$

In the region $\theta < 2T$, Tanh $(\theta/2T) \rightarrow \theta/2T$, and (9) becomes

$$E_c = (\vec{H})^2 (\mu_g{}^2 - \mu_e{}^2) \cdot \frac{1}{6kT} \tag{12}$$

which is independent of $\theta$.

Shape of the Spectrum Lines -- Relaxation Effects

In this section we will be concerned with relaxation between the electronic levels and its effect on the shape of Mössbauer spectrum lines. Figure 4A shows the position of the spectrum lines that would result from the situation illustrated in Figure 1. If the relaxation between the electronic levels were very slow, the spectrum of Figure 4B would result. On the other hand if the relaxation between the two electronic levels were very fast, the magnetic field would in effect average out, leaving only the average quadrupole interaction, so that the spectrum of Figure 4C would result. A more interesting situation occurs when the relaxation rate is intermediate between these two extremes. It is this case which we now wish to consider in more detail.

For the purpose of this section we will assume, as mentioned previously, that the electric field gradient is axially symmetric and

Figure 4

Mossbauer Spectra for Slow and Fast Electronic Relaxation

These graphs show how the Mőssbauer spectra would appear for $Tm\ Cl_3 \cdot 6H_2O$ at a temperature $T \approx \theta$ in the limits where the electronic relaxation is either infinitely slow or infinitely fast.

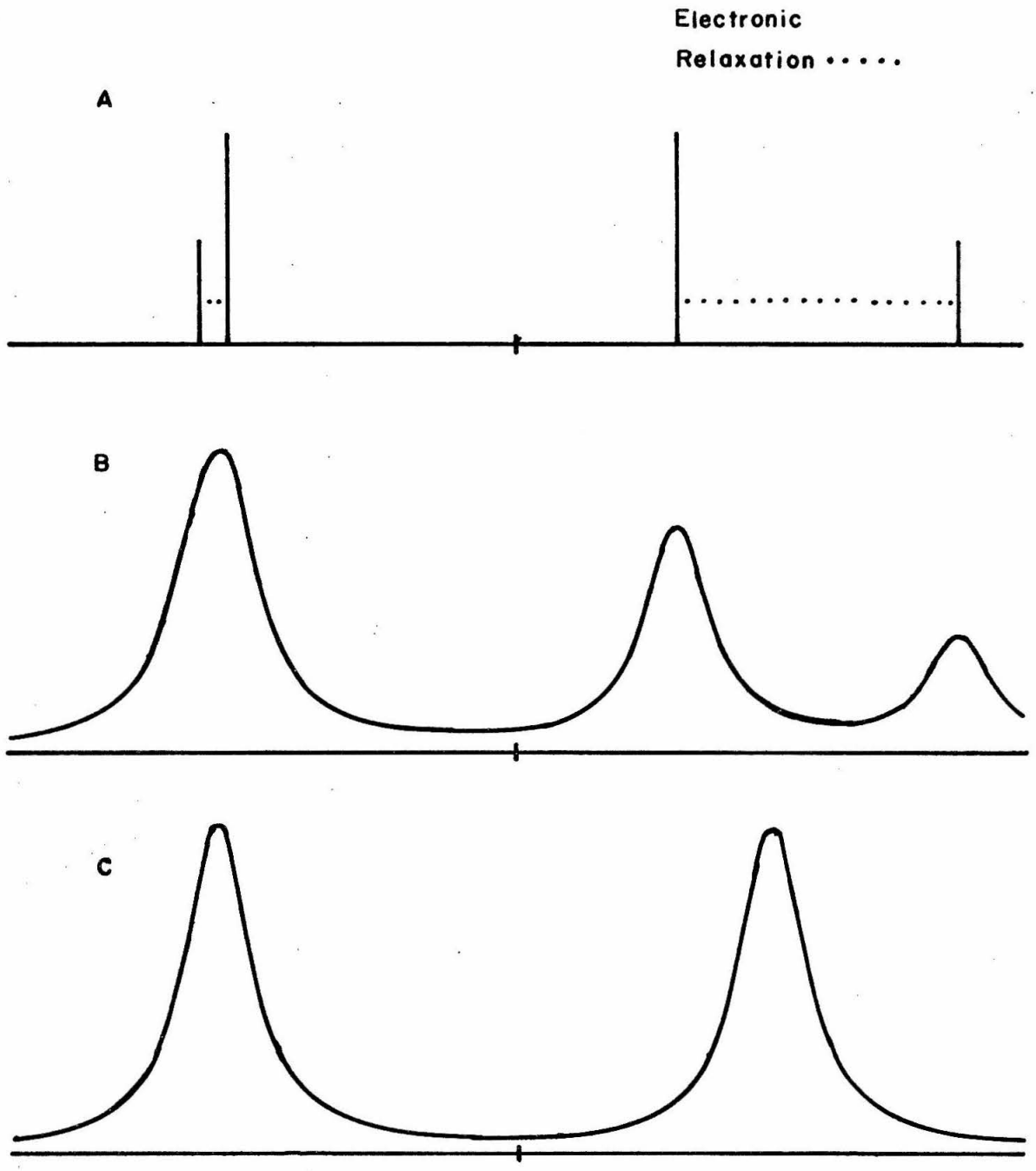


Figure 4

A. Spectrum Line Positions
B. Spectrum with Slow Relaxation
C. Spectrum with Fast Relaxation

that the vector $\langle G|\vec{J}|E\rangle$ lies along this axis. As a result of this assumption the nuclear states are eigenfunctions of $I_x$ if x is the symmetry axis. This assumption is convenient for two reasons: 1. the wavefunctions and energies are easy to compute, 2. more important, relaxation between the electronic states does not cause relaxation between nuclear states (i.e., nuclear spin flips).

Figure 2 shows the possible transitions between the various energy levels; Figure 4A shows the relaxation transitions between the spectrum lines. As can be seen, we are only concerned with pairs of spectrum lines. Anderson[9] has worked out a method of calculating the effect of relaxation on spectrum line shapes which he calls the random frequency-modulation model. We have used his model to calculate the shape of our spectra. (See Appendix V for the details of the derivation.) We hypothesize two Mössbauer spectrum lines located at $\pm \omega_0$, each with a width (FWHM) in the absence of relaxation of $2\Gamma$. (Note, this is <u>not</u> the usual definition). One line will be the spectrum line emitted (or absorbed) when the electrons are in the ground state $|G\rangle$ and the other line when in the excited state $|E\rangle$. We define $\omega_a dt$ as the probability that the electrons are in the excited state at time t + dt, given that they were in the ground state at time t. We similarly define $\omega_b$ for the reverse transition. We will <u>not</u> require that $\omega_a = \omega_b$. From these we define the auxiliary quantities

$$\omega_e = (\omega_a + \omega_b)/2$$
$$\delta = \frac{\omega_b - \omega_a}{\omega_b + \omega_a} . \qquad (13)$$

In the limit $\omega_e \gg \omega_0$ (fast, but not infinitely fast, relaxation) we have a single line which is nearly Lorentzian with its center at $-\omega_0\delta$ and with a width (FWHM) of $2\Gamma + (1 - \delta^2)\omega_0^2/\omega_e$. Due to the requirement of detailed balancing we must have

$$\omega_a/\omega_b = e^{-\theta/T} \tag{14}$$

where $k\theta$ is the difference in energy of the ground and excited electronic states. Hence we have that

$$\delta = \text{Tann } (\theta/2T) \tag{15}$$

independent of the details of the relaxation process. Consequently, we see that the center is at $-\omega_0$ Tanh $(\theta/2T)$ in agreement with the previous section, and a width of $2\Gamma + (\omega_0^2/\omega_e)\left[1 - \left(\text{Tanh } \frac{\theta}{2T}\right)^2\right]$.

As can be seen from the above, the details of the relaxation are embodied in $\omega_e$. If the relaxation is due to a spin lattice "direct" process where the transition $|G\rangle \longrightarrow |E\rangle$ is caused by the absorption of a phonon of energy $k\theta$, then $\omega_a$ is proportional to the number of phonons of energy $k\theta$. Hence the temperature dependence can be immediately written down with the help of the Planck distribution

$$\begin{aligned} \omega_a &= \frac{\omega_{SL}}{e^{\theta/T} - 1} \\ \omega_b &= \frac{\omega_{SL}\, e^{\theta/T}}{e^{\theta/T} - 1} \end{aligned} \tag{16}$$

where $\omega_{SL}$ is a constant. Hence

$$\omega_e = 1/2\ (\omega_a + \omega_b) = \omega_{SL}\left(2 \text{ Tanh } \frac{\theta}{2T}\right)^{-1} \tag{17}$$

from which we get the width

$$W_{SL} = 2\left\{\Gamma + \frac{\omega_0^2}{\omega_{SL}}\left(\text{Tanh}\,\frac{\theta}{2T}\right)\left[1 - \left(\text{Tanh}\,\frac{\theta}{2T}\right)^2\right]\right\}. \qquad (18)$$

In particular, we notice that the second term is proportional to $1/T$ at temperatures $T \gg \theta$, has a maximum at $\text{Tanh}\,(\theta/2T) = (1/3)^{1/2}$ or $T = 0.76\,\theta$, then decreases to zero at $T = 0$ (where only $|G\rangle$ is populated).

For the case of spin - spin relaxation we will assume a model where the spins of the ions are flipped in pairs, that is, we have transitions of the form $|E_i\rangle|G_j\rangle \leftrightarrow |G_i|E_j\rangle$ where $|E_i\rangle$ means that the ion at site i is in the excited state, etc. If we assume that the probability for the $i^{th}$ ion to flip is the sum of the probabilities for pair flips, summed over j, we find that the probability is given by

$$\omega_a = \sum_j{}' \omega(\vec{r}_{ij})\,\rho(E_j) \qquad (19)$$

for $|G_i\rangle \rightarrow |E_i\rangle$ where $\omega(\vec{r}_{ij})$ is the probability for the transition $|G_i\rangle|E_j\rangle \rightarrow |E_i\rangle|G_j\rangle$, given that the ions at sites i and j are in the states $|G_i\rangle$ and $|E_j\rangle$, respectively. $\rho(E_j)$ is the probability that the ion at site j is in the state $|E_j\rangle$. For a dilute crystal $\rho$ will be given by

$$\rho(E_j) = f_j\,\frac{e^{-\theta/T}}{1 + e^{-\theta/T}} \qquad (20)$$

where $f_j$ is the probability that the $i^{th}$ site is occupied by an ion of the right type (in our case, $Tm^{169}$). For random population of the lattice sites, $f_j = f$, the fractional concentration. Consequently,

(19) becomes

$$\omega_a = \frac{f\,\omega_{SS}\, e^{-\theta/T}}{1 + e^{-\theta/T}} \tag{21}$$

where

$$\omega_{SS} = \sum_j{}' \omega(\vec{r}_{ij}). \tag{22}$$

Similarly

$$\omega_b = \frac{f\,\omega_{SS}}{1 + e^{-\theta/T}} \tag{23}$$

then

$$\omega_e = 1/2(\omega_a + \omega_b) = 1/2\ \omega_{SS}\ f \tag{24}$$

from which we get the width

$$W_{SS} = 2\Gamma + 2\,\frac{\omega_0^2}{f\,\omega_{SS}}\left[1 - \left(\mathrm{Tanh}\,\frac{\theta}{2T}\right)^2\right]. \tag{25}$$

For $T \gg 1/2\ \theta$ the width is independent of temperature; as $T \to 0$, $\omega_{SS} \to 2\Gamma$. We see also that the second term varies inversely as the concentration.

Finally, we might consider the effect that the neighboring atoms may have directly on the hyperfine structure. That is, the magnetic moments on the neighboring ions may in effect change $\omega_0$. If this were the case, then roughly both $\omega_0$ and $\omega_e$ would be proportional to the concentration so that the second term in Eq. (25) would vary directly, instead of inversely, as the concentration. We have made rough calculations which indicate that this type of broadening becomes appreciable only near 100% Tm in $TmCl_3 \cdot 6H_2O$, and is

still small compared to $\Gamma$. It does seem important for the sulphate.

In order to estimate $\omega_{SS}$, we will use a simple model. We take two ions which are separated by a distance $r_{12}$, and which have two states $|E\rangle$ and $|G\rangle$. The states have the matrix elements:

$$\langle G|\vec{J}|G\rangle = 0 \qquad \langle E|\vec{J}|E\rangle = 0 \qquad \langle G|\vec{J}|E\rangle \neq 0 \tag{26}$$

The states of the combined system can be written

$$|A\rangle = |E_1, G_2\rangle \qquad |B\rangle = |G_1, E_2\rangle$$
$$|C\rangle = |G_1, G_2\rangle \qquad |D\rangle = |E_1, E_2\rangle \tag{27}$$

States A and B are degenerate while C and D lie above and below with a total separation of $2k\theta$. If we now let the ions interact through the dipole-dipole interaction we have only two non-zero matrix elements:

$$\hbar\omega_{dd} = \langle A|H_{dd}|B\rangle$$
$$\hbar\omega'_{dd} = \langle C|H_{dd}|D\rangle \; . \tag{28}$$

Here we are interested only in the first of these matrix elements, since these are the only pair transitions which conserve energy. The eigenstates now become:

$$|1\rangle \equiv 1/\sqrt{2}\,(|A\rangle + |B\rangle) \qquad E_1 = \hbar\omega_{dd}$$
$$|2\rangle = 1/\sqrt{2}\,(|A\rangle - |B\rangle) \qquad E_2 = -\hbar\omega_{dd} \tag{29}$$

If we now require that at t = 0 our system be in state $|A\rangle$, we have the following time-dependent wavefunction

$$\begin{aligned}\psi(t) &= 1/\sqrt{2}\,(|1\rangle\, e^{i\omega_{dd}t} + |2\rangle\, e^{-i\omega_{dd}t}) \\ &= |A\rangle \cos\omega_{dd}t + |B\rangle \sin\omega_{dd}t.\end{aligned} \tag{30}$$

We may interpret this as a relaxation between A and B with a relaxation time $1/\omega_{dd}$.

The dipole-dipole interaction may be written as[10]:

$$H_{dd} = \mu_0\beta^2\, \langle J||\Lambda||J\rangle^2 \left[\frac{\vec{J}_1\cdot\vec{J}_2}{r_{12}^3} - 3\,\frac{(\vec{J}_1\cdot\vec{r}_{12})(\vec{J}_2\cdot\vec{r}_{12})}{r_{12}^5}\right]. \tag{31}$$

Since we are interested only in an order of magnitude estimate we will drop the second term. We then get

$$\hbar\,\omega_{dd} = \mu_0\beta^2\, \langle J||\Lambda||J\rangle^2\, \frac{\langle G|\vec{J}|E\rangle^2}{r_{12}^3}\,. \tag{32}$$

## EXPERIMENTAL EQUIPMENT

The 8.4 keV gamma transition in Tm 169 was used for all the Mössbauer experiments. Er 169 decays with a half life of about nine days by beta decay to the first excited level of Tm 169, which is $3/2^+$. The ground state of Tm 169, which is the only stable thulium isotope, is $1/2^+$.

Our absorbers were made of $TmCl_3 \cdot 6H_2O$, $Tm_2(SO_4)_3 \cdot 8H_2O$, and Tm O I as well as thulium chloride and sulphate diluted with the corresponding salt of yttrium. Yttrium was used because $Y^{3+}$ is diamagnetic: it has only closed shells of electrons. Furthermore, it is chemically very similar to Thulium: the difference in ionic radius between $Tm^{3+}$ and $Y^{3+}$ is about 2%. To prepare the chloride absorbers, measured amounts of $Tm_2O_3$ and $Y_2O_3$ were dissolved in warm 3N HCl. The acid solution was then placed in a desiccator containing $P_2O_5$ as a desiccant. The solution was dried overnight with a forepump keeping the desiccator evacuated. In this period small white crystals were formed. These crystals were observed to be slightly deliquescent; that is, on humid days, when the relative humidity was above 60% or so, the crystals condensed enough water vapor in which to dissolve themselves. When the humidity dropped to 40% or so, the crystals dried out again. It was also observed that crystals left in the desiccator for several days lost some of their crystal water: when such crystals were allowed to stand in the air (relative humidity about 40%) they would gain weight for about half an hour, after which the weight remained constant. Before they regained

their crystal water, such crystals also showed broadened Mössbauer spectra lines with a smaller quadrupole splitting.

The sulphate absorbers were prepared by dissolving mixtures of commercially available yttrium and thulium sulphates in water and then drying the resulting solution. The Tm O I was prepared according to procedures described by Asprey[10a]. The chloride and sulphate absorbers themselves were made by mixing about 100 mg of the finely ground powder with an equivalent weight of wax and pressing the mixture into a one-inch diameter disc between mylar films. The oxy-iodide absorbers were made by dispersing the powdered TmOI with about 200 mg of diamond dust. This mixture was then clamped between two thin beryllium discs.

The source, velocity transducer, and electronics are essentially the same as those described elsewhere[11]. For most of the experiments a parabolic velocity reference signal (a twice-integrated square wave) was used. The error signal, which is the difference between the actual velocity of the source and the reference signal is shown in Figure 5. for the chloride experiments.

The cryostat design, the essential parts of which are shown in Figure 6, was used primarily because of the accuracy with which the temperature of the absorber could be determined and controlled. Since the absorber was immersed directly in the liquid Helium, the temperature of the absorber could easily be determined by measuring the vapor pressure of the Helium. The temperature could be reduced to 1.0°K by pumping on the helium bath. One added convenience of the cryostat design was that the absorber holder could be easily removed

Figure 5

Velocity Reference Signal and Error Signal

This Figure shows the time dependence of these signals, which characterize the operation of the velocity transducer. These were the signals recorded for the chloride experiments. The signals for the other experiments were similar. The zero point of the velocity scale of the error signal may not be exactly correct.

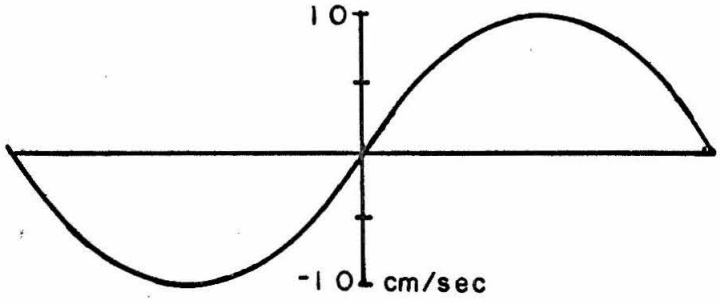


Velocity Reference Signal

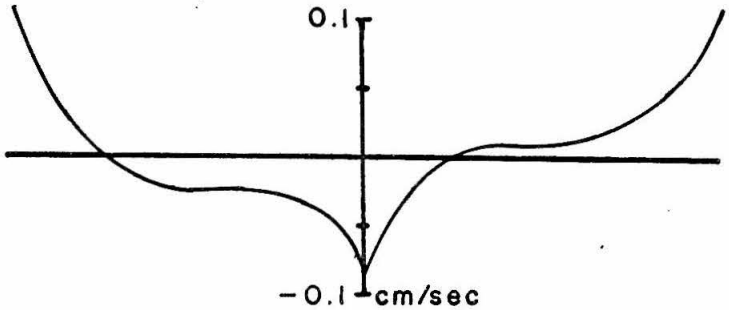


Velocity Error Signal
(Actual – Reference)

Figure 5

Figure 6

Cryostat Schematic

This figure illustrates schematically the construction of the cryostat used for the low temperature experiments. The upper part, including the helium and nitrogen reservoirs, is a modular dewar built by Andonian Associates.

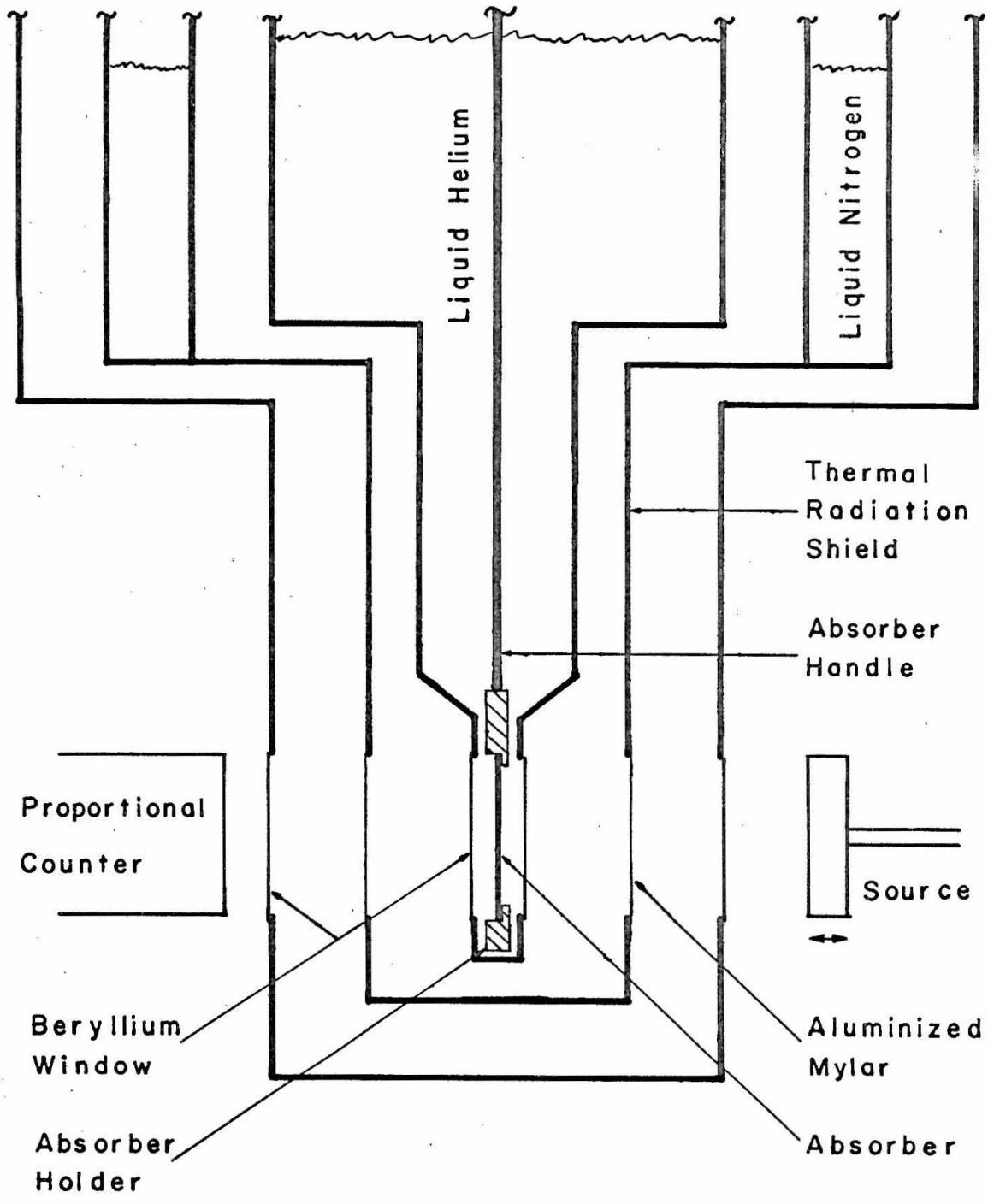


Figure 6

CRYOSTAT SCHEMATIC

or inserted from the top of the cryostat without warming the cryostat itself above 4.2°K. Consequently, absorbers could be interchanged in a few minutes with a loss of only a few c.c's of liquid helium.

For the high temperature TmOI experiments, an oven was used which permitted the absorber to remain immersed in an inert gas, since contact with the atmosphere would decompose the oxyiodide. The temperature was measured with a Chromel-Alumel thermocouple. The oven was heated by a coil of Nichrome wire surrounding the region occupied by the absorber.

In some of the experiments a problem arose which we believe to be due to some time constants in the pulse height analysing circuits and the associated amplifiers. We believe we can correct for this. The non-resonant background is not a flat function of velocity but slants. By measuring the background in the absence of the absorber - indeed, in the absence of everything but the source and the proportional counter - we found that the background was a linear function of velocity, though the amount of slant varied from experiment to experiment. If this problem does not otherwise affect the spectrum, then it is easy enough to correct for it in our least squares analysis of the data.

The analysis of the data was greatly facilitated by using a least squares fitting program. As an illustration, the standard deviation of the position of a spectrum line 2 cm/sec wide was typically 0.01 cm/sec. If the position were determined "by eye" the error limit would be at least 0.1 cm/sec - ten times larger.

The data from each experiment were fit to two Lorentzians of

equal area with a slanting background. Explicitly, the function is:

$$f(v) = \left[\alpha - \sum_{i=1,2} \frac{\beta W_i}{(v - v_i)^2 + W_i^2}\right](1 + \gamma v). \quad (33)$$

The variable parameters are:

| | |
|---|---|
| $\alpha$ | the non-resonant background at zero velocity |
| $\beta$ | proportional to the area of the peak; it is equal to the height multiplied by the half-width $W_i$ |
| $\gamma$ | proportional to the slope of the background |
| $v_i$ | center of the $i^{th}$ peak |
| $W_i$ | half-width of the $i^{th}$ peak (1/2 FWHM). |

In particular, it should be noticed that the areas of both peaks were constrained to be equal. This was done since the broadening should not affect areas of the peaks. The results of least squares analysis are presented in Table I for the chloride and sulphate spectra.

TABLE I

The results of the least-squares analysis of selected chloride and sulphate data are presented here. See the text for an explanation of the parameters (the parameter $\gamma$ is not tabulated). The velocity units are cm/sec. The temperature T is in degrees Kelvin; the concentration f is the atomic fraction of thulium; the thickness of the absorber $\tau$ is in $mg/cm^2$ of thulium. "fig." refers to the figure where the data are plotted. Single line sources of Tm in Er $F_3$ heated to about $275^oC$[13] were used for all of the experiments. There was some variation of the width of the line for different sources. This is reflected in the $\sim$ 60% larger value of $W_1$ for Tm $Cl_3 \cdot 6H_2O$ at $1.13^oK$, $130^oK$, $195^oK$.

Table IA Tm in $YCl_3 \cdot 6H_2O$

| T $^oK$ | f | $\tau$ $mg/cm^2$ | fig. | $\alpha$ $x10^6$ | $\beta$ $x10^3$ | $W_1$ cm/sec | $W_2$ cm/sec | $V_1$ cm/sec | $V_2$ cm/sec |
|---|---|---|---|---|---|---|---|---|---|
| 1.13 | 1.0 | 6.0 | 7A | 0.97 | 67 | 1.57 | 1.64 | -7.21 | 6.06 |
| 1.85 | 1.0 | 6.0 | 7B | 3.38 | 154 | 1.01 | 1.13 | -7.22 | 6.47 |
| 4.2 | 0.06 | 4.6 | 9A | 18.7 | 101 | 0.86 | 1.5 | -7.35 | 7.0 |
| 4.2 | 0.09 | 1.5 | 9B | 3.15 | 55 | 0.88 | 1.28 | -7.38 | 6.97 |
| 4.2 | 0.17 | 1.6 | | 4.63 | 82 | 0.89 | 1.16 | -7.33 | 6.97 |
| 4.2 | 0.25 | 2.1 | 9C | 3.95 | 69 | 0.90 | 1.01 | -7.30 | 6.95 |
| 4.2 | 0.33 | 3.7 | | 2.09 | 60 | 0.90 | 0.93 | -7.36 | 7.01 |
| 4.2 | 0.50 | 4.6 | | 2.20 | 110 | 0.94 | 0.95 | -7.34 | 7.01 |
| 4.2 | 1.0 | 6.0 | 7C,9D | 7.13 | 299 | 0.95 | 1.04 | -7.30 | 6.97 |
| 130 | 1.0 | 6.0 | 11C | 2.83 | 162 | 1.64 | 2.5 | -6.62 | 6.71 |
| 195 | 1.0 | 6.0 | 11B | 2.45 | 124 | 1.69 | 3.3 | -4.13 | 4.0 |
| 295 | 0.17 | 1.6 | | 5.61 | 79 | 1.05 | 1.66 | -2.13 | 2.12 |
| 295 | 0.33 | 3.7 | | 3.23 | 146 | 1.11 | 1.52 | -2.12 | 2.16 |
| 295 | 1.0 | 6.0 | 11A | 2.24 | 95 | 1.02 | 1.44 | -2.12 | 2.15 |

Table I B Tm in $Y_2(SO_4)_3 \cdot 8H_2O$

| | | | | | | | | | |
|---|---|---|---|---|---|---|---|---|---|
| 1.2 | 0.048 | 1.3 | | 2.59 | 19 | 1.0 | 2.7 | -7.36 | 5.3 |
| 1.2 | 0.18 | 3.9 | 12B | 2.09 | 48 | 1.07 | 2.3 | -7.30 | 6.2 |
| 4.2 | 0.048 | 1.3 | 12A | 4.15 | 24 | 0.9 | 2.8 | -7.4 | 6.2 |
| 4.2 | 0.18 | 3.9 | 12C | 2.35 | 53 | 1.08 | 2.6 | -7.44 | 7.0 |
| 4.2 | 1.0 | 11.0 | 12D | 2.93 | 175 | 1.7 | 10 | -7.46 | 6 |
| 80 | 1.0 | 9.3 | 13B | 8.98 | 414 | 1.84 | 9.5 | -7.18 | 5.8 |
| 295 | 1.0 | 9.3 | 13A | 8.66 | 245 | 1.22 | 1.47 | -1.72 | 1.75 |

## EXPERIMENTAL RESULTS

### Shift of the Center of Gravity

Figure 7 shows Mössbauer spectra of Tm $Cl_3 \cdot 6H_2O$ at various temperatures between $1^oK$ and $4.2^oK$. The solid line is the result of the least-squares fit. The center of gravity of the spectrum was then taken to be halfway between the centers of the two peaks. The positions of the centers of gravity have been plotted versus temperature in Figure 8. The solid lines are plots of Eq. (2) for several values of $\theta$, adjusting $E_0$ in each case to obtain the best fit to the data. The best fit is obtained with $\theta = 1.6^oK \pm 0.25 = 1.1\ cm^{-1} \pm 0.17$, and $E_0 = 2.1 \times 10^{-3}\ cm^{-1} \pm 0.3 \times 10^{-3}$. The error quoted here is purely statistical; as can be seen from the graph any appreciable systematic errors could throw this off considerably. If we wished to determine $\theta$ more accurately we should extend the measurements to lower temperatures, where the curves are more sensitive to $\theta$. However, this is not possible with our present equipment. We can, however, determine with good accuracy the quantity $\sqrt{|E_0 k\theta|} = 0.0480\ cm^{-1} \pm 0.0007$. From Eq. (8) we get

$$E_0\, k\, \theta = 1/3\, M^2 \left|\langle G|\vec{J}|E\rangle\right|^2 \left[g_g^{\,2} I_g(I_g + 1) - g_e^{\,2} I_e(I_e + 1)\right] . \tag{34}$$

If we use the magnetic field measured in Tm metal[12] to obtain values for gM, assuming that the field comes entirely from the 4f electrons with $J_z = 6$ we get

Figure 7

$Tm\ Cl_3 \cdot 6H_2O$ at Low Temperatures

This figure illustrates the shift of the center of gravity of the spectra of the chloride absorbers at low temperatures. The solid curves are the least-squares fit to the data. The parameters for these curves are in Table I. The straight slanted line represents the non-resonant background computed in the least-squares analysis. The vertical dotted lines are the computed centers of the spectrum peaks. The statistical standard deviation of the position of the center of a peak was typically 0.01 cm/sec or less; this is about the size of one of the small dots. Single line sources of Tm in $Er\ F_3$ heated to about 275°C were used for all of the these experiments. Both peaks in 7C are about 50% broader than the peaks of Figures 7A and 7B. This is due to using a source with a broader line width for Figure 7C. The same source was also used for the data shown in Figures 11B and C.

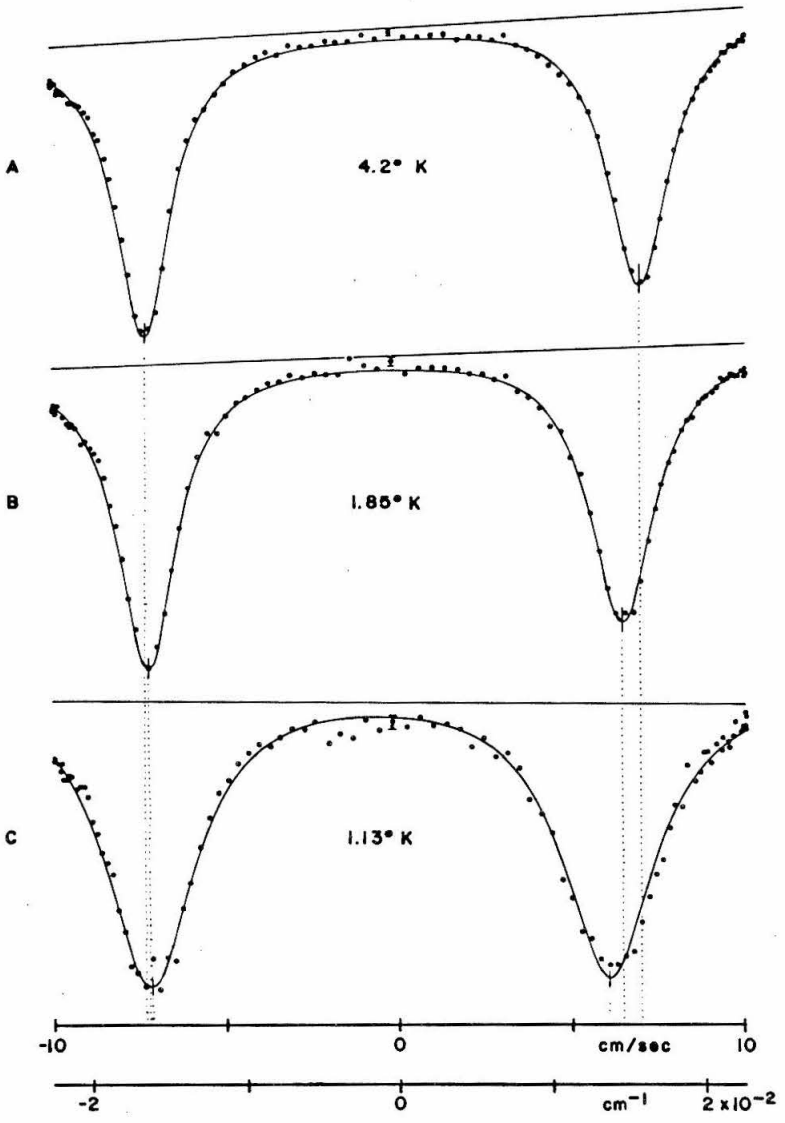


Figure 7
$TmCl_3 \cdot 6H_2O$ AT LOW TEMPERATURES

Figure 8

Center of Gravity of Mossbauer Spectra of $Tm\ Cl_3 \cdot 6H_2O$ as a Function of Temperature

The experimental points shown here include some results from thulium diluted by yttrium. The solid lines represent curves of $E_0 Tanh(\theta/2T)$ for several values of $\theta$; in each case $E_0$ was chosen to fit the experimental points best. The curve for $\theta = 1.1\ cm^{-1}$ represents the best fit to the experimental points.

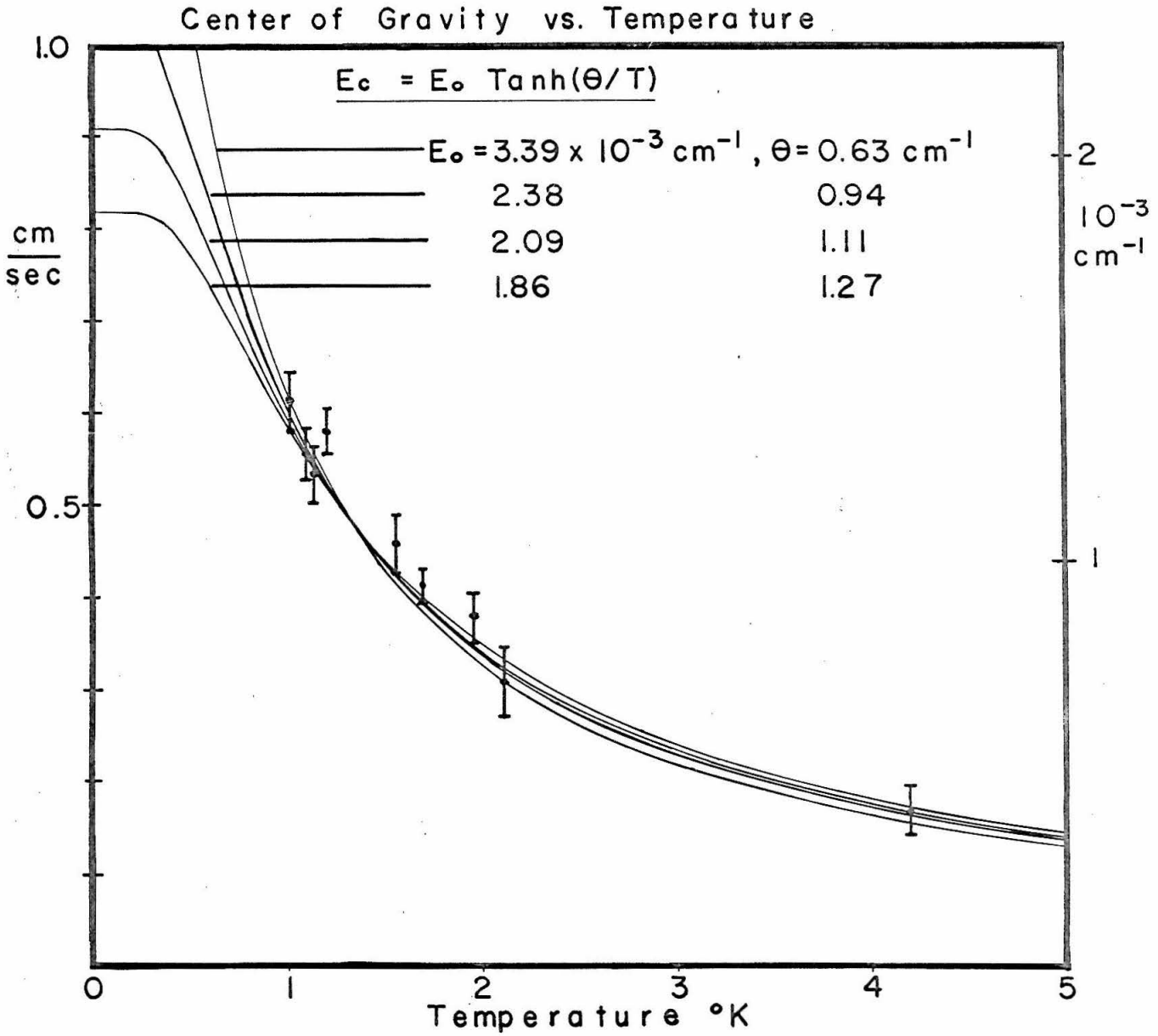
Center of Gravity vs. Temperature
Ec = Eo Tanh(θ/T)
Eo = 3.39 x 10^-3 cm^-1 , θ = 0.63 cm^-1
2.38 0.94
2.09 1.11
1.86 1.27
1.0
0.5
cm/sec
2
1
10^-3 cm^-1
0
1
2
3
4
5
Temperature °K

Figure 8

$$g_g M = -\ 1.23 \times 10^{-2}\ \text{cm}^{-1}$$
$$g_e M = 0.94 \times 10^{-2}\ \text{cm}^{-1}\ . \qquad (35)$$

For $Tm^{169}$, we find:

$$|\langle G|\vec{J}|E\rangle|^2 = 30.1. \qquad (36)$$

This should be compared with the value of 34.8 calculated from the CEF data. This is fairly good agreement, considering the approximations and assumptions made in both calculations.

Although the shape of the spectrum lines was affected by diluting the thulium with yttrium, as we shall see in the next section, the shift of the center of gravity is not affected by the dilution within the accuracy of our measurements. In fact, the points in Figure 8 contain results not only of the undiluted thulium chloride but also of the thulium chloride diluted by yttrium chloride.

Asymmetric Line Broadening

Figure 9 shows Mössbauer spectra of Tm in $Y\,Cl_3 \cdot 6H_2O$ for several different concentrations of Tm. Since $\omega_0$, the separation of the component spectrum lines in the absence of relaxation, in Eq. (25) is different for the two observed peaks, the difference in width of the observed peaks is assumed to be due to relaxation. In Figure 10 the difference in widths of the two peaks is plotted against 1/f, the fractional concentration. The solid line is the best fit of the data to a straight line. In Eq. (25) $(\text{Tanh}\ \theta/2T)^2$ is less than 0.05 at $4.2^{\circ}K$ and is more likely to be about 0.01;

Figure 9

Tm in Y $Cl_3 \cdot 6H_2O$ at $4.2^{\circ}K$

This figure illustrates the asymmetrical broadening of the spectrum peaks with decreasing thulium concentration.

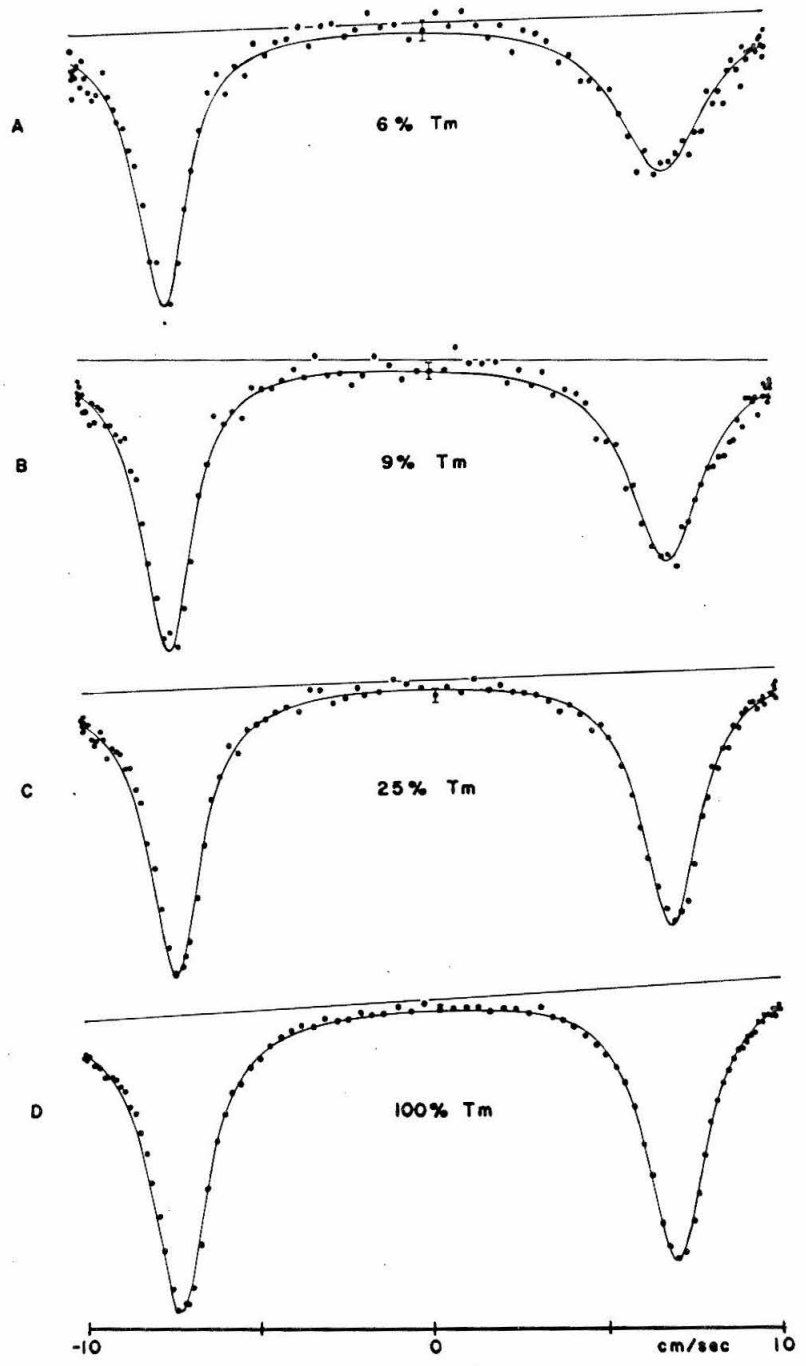


Figure 9

Tm in $YCl_3 \cdot 6H_2O$ at 4.2° K

Figure 10

Line Width Asymmetry as a Function of Thulium Concentration

The difference of the widths (FWHM) of the two asymmetrical lines in Figure 9 is plotted versus the reciprocal of the fractional atomic concentration of Tm in $YCl_3 \cdot 6H_2O$. The experimental points were all measured at $4.2^{o}K$. The solid line is the best fit of the data to a straight line.

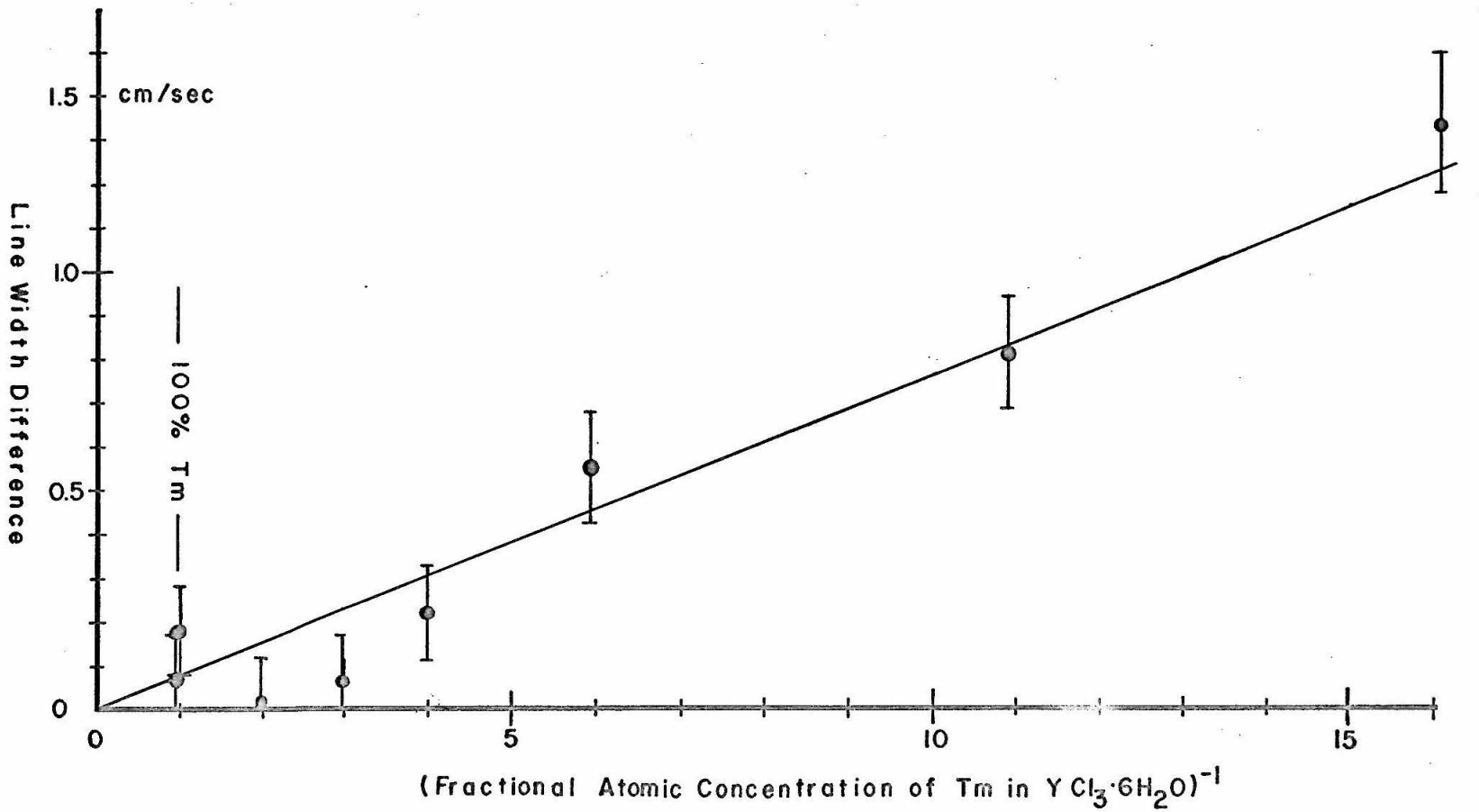


Figure 10

LINE WIDTH ASYMMETRY AS A FUNCTION OF THULIUM CONCENTRATION

consequently we can neglect it. The best fit is then obtained with

$$\frac{\omega_{0_1}^2 - \omega_{0_2}^2}{2\pi\, c\, \omega_{SS}} = (8.6 \pm 1.1)\ 10^{-5}\ \text{cm}^{-1} \qquad (37)$$

where the subscripts 1 and 2 refer to the two spectrum peaks. Using perturbation theory to compute $\omega_0$ in a manner similar to Appendix IV we get

$$\hbar\,\omega_0 = \frac{(\vec{H})^2}{k\,\theta}\,(g_g^{\,2} m_g^{\,2} - g_e^{\,2} m_e^{\,2}). \qquad (38)$$

Using our value of $\vec{H}$ computed from the shift of the center of gravity, and $k\theta = 1.0\ \text{cm}^{-1}$ we may compute a value for $\omega_{SS}$:

$$\frac{\omega_{SS}}{2\pi\, c} = (0.27 \pm 0.04)\,\text{cm}^{-1} \qquad (39)$$

or

$$1/\omega_{SS} = 2.0 \times 10^{-11}\ \text{sec.}$$

The error quoted here is the statistical error in the measurement of the effective internal field and of the line broadening; it does not include any error in $\theta$; $k\theta$ may be as small as $0.1\ \text{cm}^{-1}$. ($k\theta = 0.5\ \text{cm}^{-1}$ would make $\omega_{SS}/2\pi c = 1\ \text{cm}^{-1}$.)

For $Tm^{3+}$ $\langle J||\Lambda||J\rangle = 7/6$ [10]; from previous results we know $\langle\vec{J}\rangle^2 = 30$; for r we will use the distance to the nearest neighbor, $r = 6.5$ Å. Hence, from Eq. (32) we get

$$\omega_{dd}/2\pi c = 0.064\ \text{cm}^{-1}. \qquad (40)$$

When the second term of Eq. (31) is included and the result summed over the six nearest thulium neighbors, which form a rough octahedron,

the result in Eq. (40) is increased by a factor between 4 and 8, depending on the exact orientation of $\langle G|\vec{J}|E\rangle$. Summation over the rest of the lattice will increase this further. In any case, the value in (40) is increased so that it is the same order of magnitude as (39).

Thulium Chloride at Higher Temperatures

In Figure 11 some Mössbauer spectra at higher temperatures are shown. As expected[13], the quadrupole splitting decreases as the temperature increases. The more striking result is that the broadening of the spectrum lines becomes more asymmetrical as the temperature increases. We attribute this phenomena to the magnetic interaction of the nucleus with the higher lying, nearly degenerate pair of levels mentioned in the description of the 4f levels. The calculated splitting of these levels is smaller ($\sim$ 0.1 $cm^{-1}$) than for the lowest pair so that the interaction is correspondingly larger. However, because the size of the splitting of the higher pair is relatively more sensitive to the variation of the CEF parameters, we have not tried to use Anderson's theory to calculate the shape of the spectrum, also the situation is complicated considerably by the fact that all of the 13 CEF levels are populated. At these temperatures, the electronic relaxation will be primarily spin-lattice relaxation, which is independent of concentration. This independence was verified by our experiments.

Thulium Sulphate Results

Mössbauer spectra of $Tm_2(SO_4)_3 \cdot 8H_2O$ and Tm in $Y_2(SO_4)_3 \cdot 8H_2O$ are shown in Figures 12 and 13. In a general sense these spectra are

Figure 11

$Tm\ Cl_3 \cdot 6H_2O$ at Higher Temperatures

This figure illustrates the temperature dependence of the asymmetrical broadening of the spectrum peaks (compare also Figure 7).

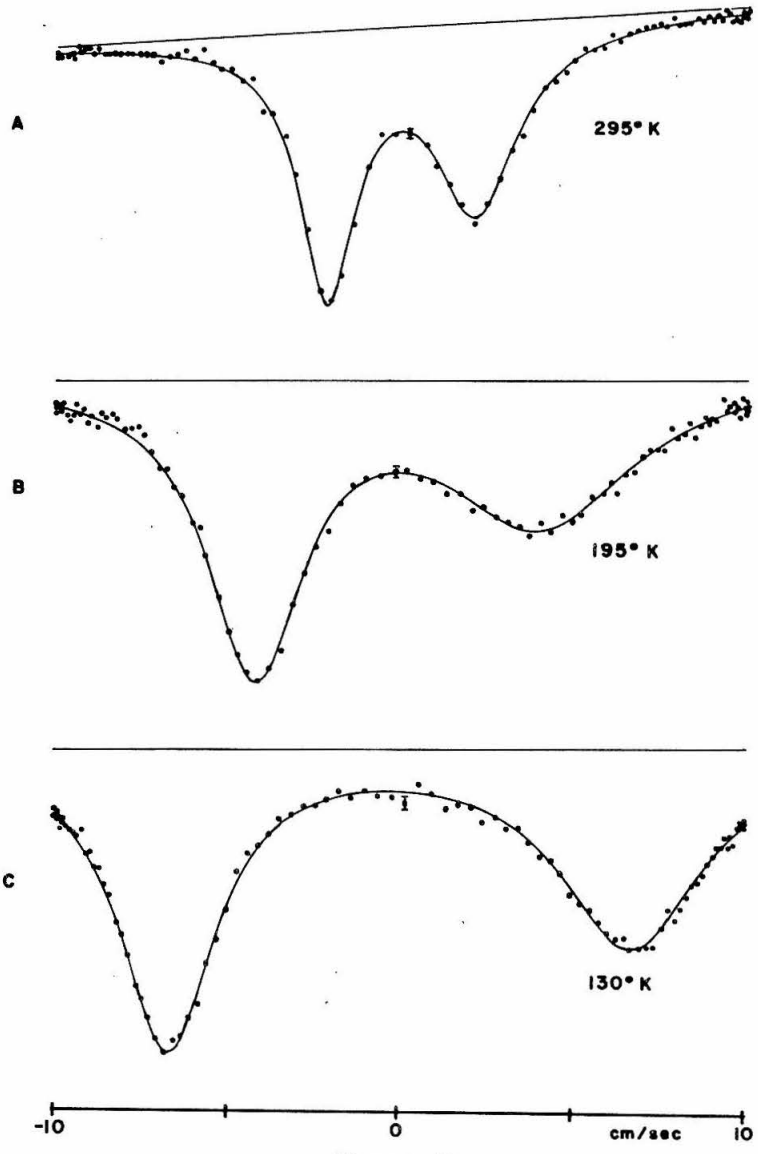


Figure 11

$Tm\,Cl_3 \cdot 6H_2O$ AT HIGHER TEMPERATURES

Figure 12

Tm in $Y_2(SO_4)_3 \cdot 8H_2O$ at Low Temperatures

This figure illustrates both the concentration dependence of the asymmetrical broadening (A,B,D) and the temperature dependent shift of the center of gravity, which is best seen in the diluted absorbers (B,C).

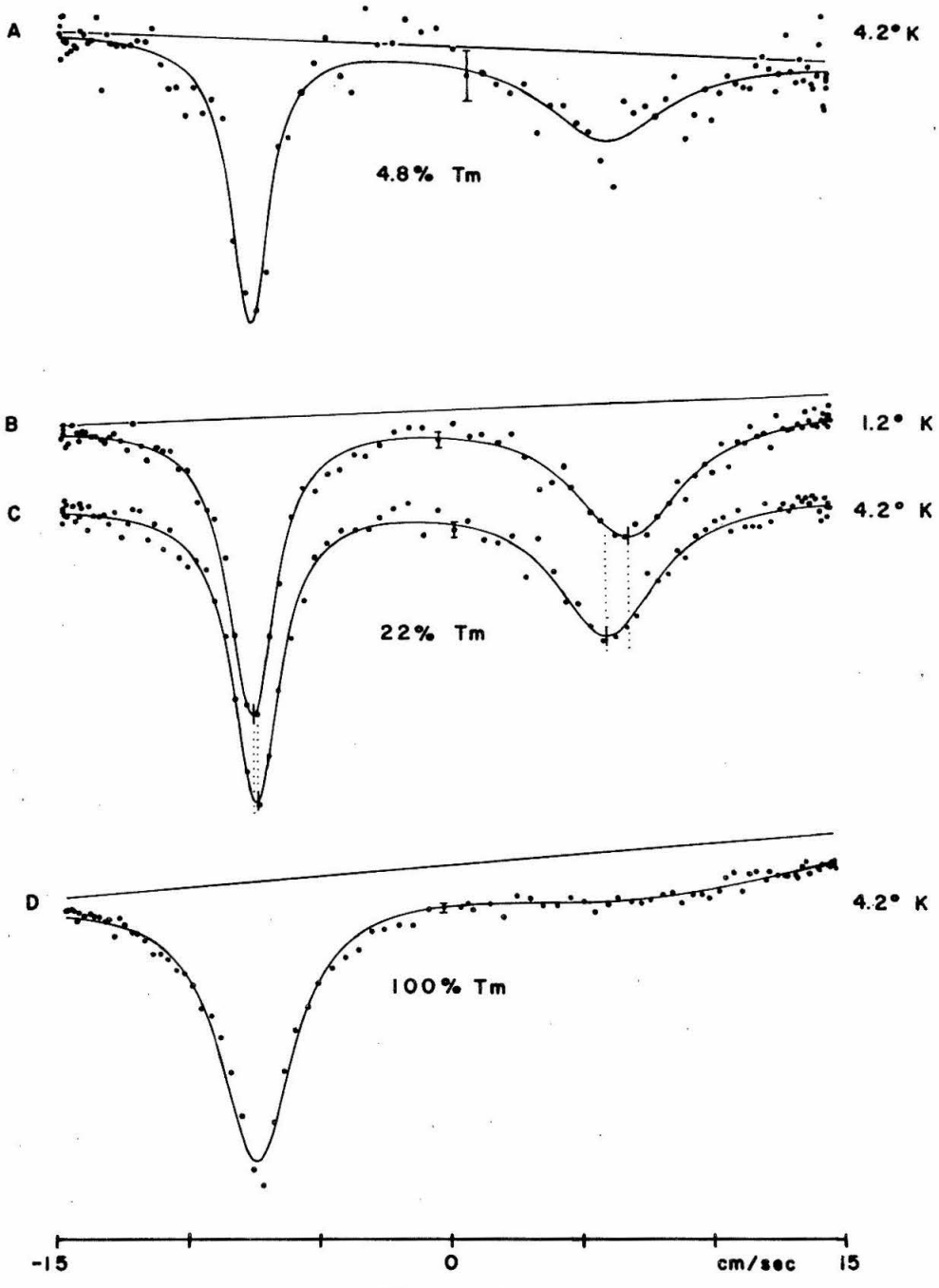


Figure 12

Tm IN $Y_2(SO_4)_3 \cdot 8H_2O$ AT LOW TEMPERATURES

Figure 13

$Tm_2(SO_4)_3 \cdot 8H_2O$ at Various Temperatures

This figure shows the temperature dependence of the asymmetrical broadening in the absorbers of thulium sulphate. Note that at low temperatures the broadening is much more pronounced than in the thulium chloride.

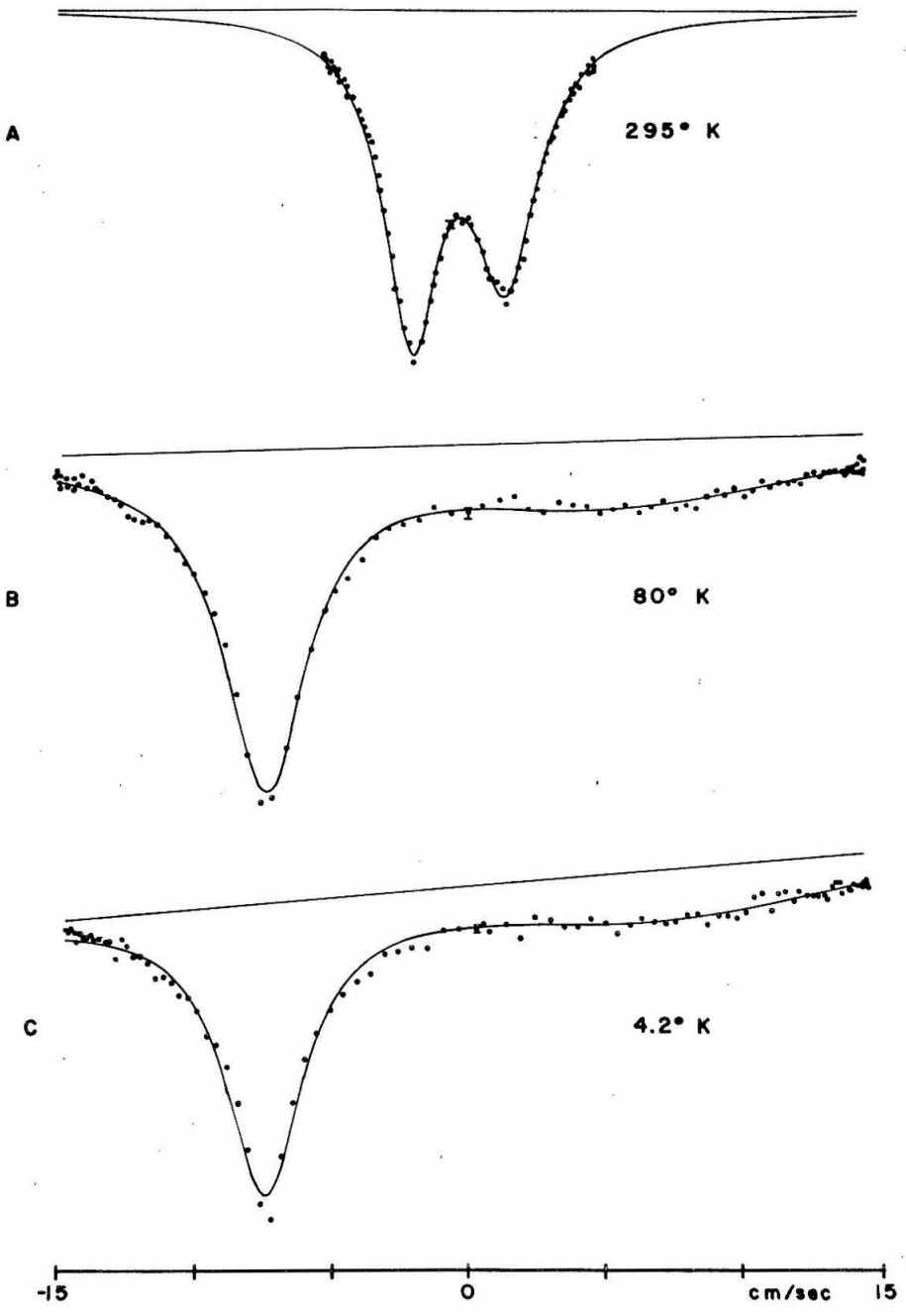


Figure 13

$Tm_2(SO_4)_3 \cdot 8H_2O$ AT VARIOUS TEMPERATURES

similar to those of the chloride. In particular, as can be seen by comparing Figures 12B and 12C, there is a shift of the center of gravity nearly the same as in the chloride. This shows that the matrix element $\langle E|\vec{J}|G\rangle$ is about the same size in the sulphate as in the chloride. On the other hand the asymmetry of the line broadening is much more pronounced and shows a different concentration dependence. For high concentration the difference in line widths increases with increasing concentration, whereas in the chloride the opposite is true. We attribute this to be evidence that the magnetic moments of the surrounding ions are directly influencing the hyperfine structure. That is, due to the magnetic interaction with the surrounding ions, the hyperfine levels, in the absence of relaxation effects, are spread into a band of levels and $\omega_0$ in Eq. (25) can now be replaced by $\omega_0'$, the width of this band. Since the width of this band is proportional to the concentration we would expect that the difference of the spectrum line widths would be proportional to the concentration until the concentration decreases enough to where $\omega_0' \approx \omega_0$. At this concentration $\omega_0$ becomes more important and the line width difference increases inversely as the concentration decreases, similar to the chloride behavior.

We have made some rough calculations which indicate that the difference between the concentration dependence of the chloride and sulphate Mössbauer spectra can be explained if the CEF splitting, $k\theta$, of the two lowest sulphate electronic levels is smaller than that of the chloride, and the magnetic dipole interaction between thulium ions is stronger in the sulphate than in the chloride.

Thulium Oxyiodide Results

Mössbauer spectra of thulium oxyiodide at several temperatures are shown in Figure 14. Since the symmetry of the oxyiodide is $C_{4v}$ (a four-fold axis of rotation with parallel mirror planes) there will be three degenerate levels (not just nearly degenerate) in the 4f level structure. Consequently we would expect stronger magnetic hyperfine interactions, producing a more asymmetric line broadening.

Figure 14

Tm OI

This Figure shows Mössbauer spectra of Tm OI absorbers at several temperatures. A least-squares fit to these curves has not yet been attempted. However we interpret the room temperature spectrum (C) as consisting of two peaks located at about ± 3 cm/sec with the peak at + 3 cm/sec being two or three times broader. At higher temperatures the splitting of these peaks decreases. The small dip on the left side of the room temperature spectrum is probably a fluke, since it did not appear in other room temperature spectra.

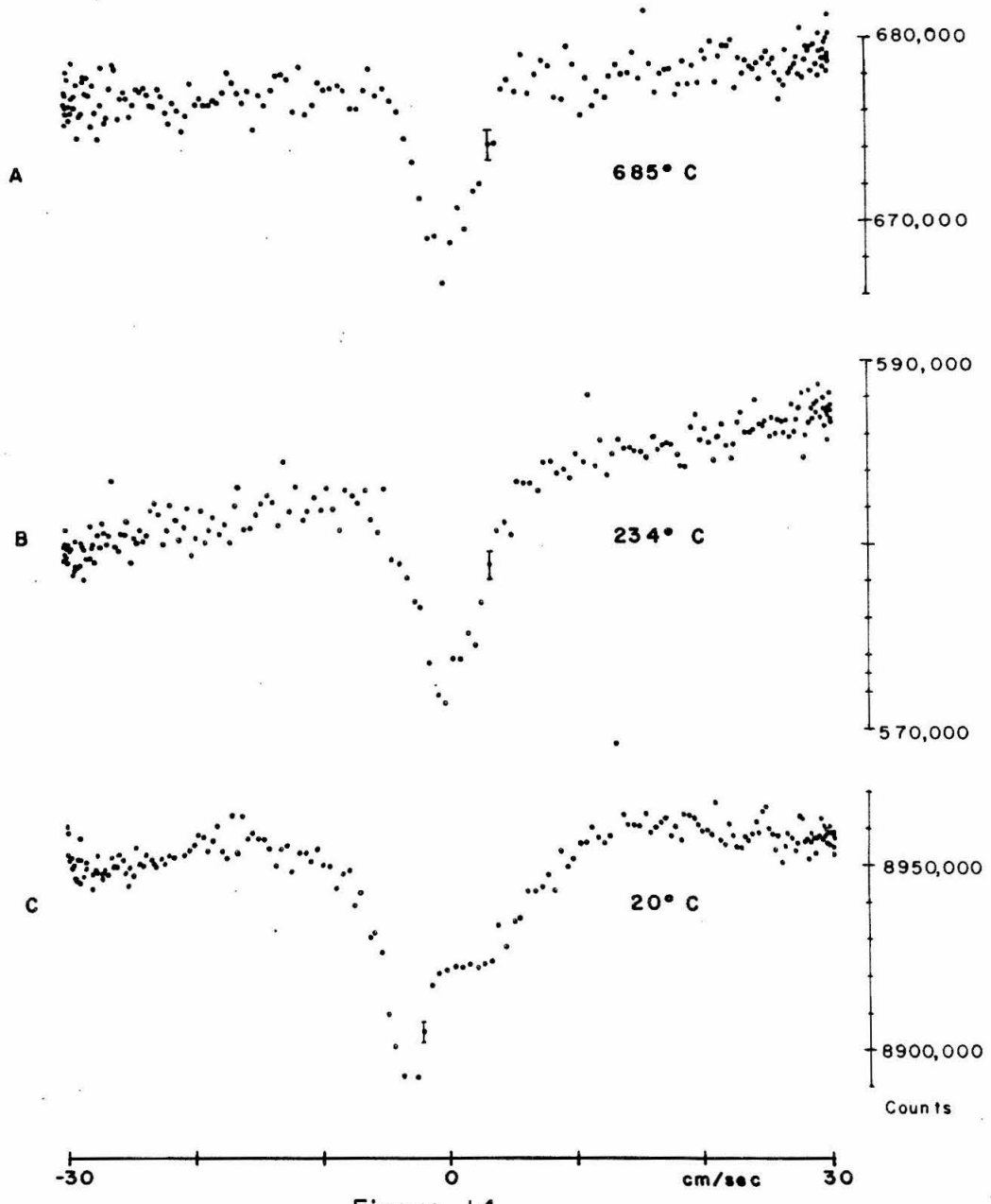


Figure 14

Tm OI

## SOURCES OF SYSTEMATIC ERROR

Since our experiments involve measuring positions and widths of lines to an accuracy of a fraction ( $\sim$ 5%) of the line width, or for that matter, a fraction of the instrumental "resolving power", we should devote some attention to possible sources of error in our measurements. Some typical velocities were: the range of velocities covered was usually from - 10 cm/sec to + 10 cm/sec; the separation between the two peaks was about 15 cm/sec; the width of a peak was about 2 cm/sec (FWHM); the instrumental resolving power (velocity increment per channel of the multi-channel analyser) in the region of a peak was about 0.2 cm/sec.

There were several sources of error which may be generally called velocity errors- errors associated with the motion of the source: The most obvious is the calibration of the drive itself. The drive is calibrated by measuring the spectrum of metallic $Fe^{57}$ at room temperature. This method, we feel, is accurate to about 1/2 %. Experience has shown that the calibration changes by less than 1/4 % per month, which is a typical span for a series of experiments. Since this error is the same for a series of experiments we may account for its effect by quoting a 1/2 % error in our end results; other sources of non-systematic error are generally several times larger. A second type of velocity error is due to the fact that the motion of the source is not exactly what it is thought to be. The source does not follow the reference signal exactly. Assuming that the source is rigidly connected to the pick-up coil, then we can measure this error; a

typical error signal is shown in Figure 5. Also, due to the fact that the integrating circuits used to produce the reference signal do not integrate perfectly, there is a certain amount of error in the reference signal. From our measurements of $Fe^{57}$ calibration spectra we believe this error to be rather small. One important point to realize about these errors is that they are all symmetric: If the two peaks were symmetric, these errors would not produce any asymmetry. Consequently, in our measurements of the difference of the widths of the peaks or of the center of gravity, these errors cancel out in lowest order; their effect will be a (small) percentage of the result.

A second type of error arose, as mentioned before, due to the slanted non-resonant background. We believe that this was not an appreciable source of error in the center-of-gravity measurements due to the internal consistency of a number of measurements on absorbers which should have in other respects given identical results. On the other hand, there is some evidence that the measurement of the widths was affected. For this reason the error limits on these measurements were increased over the statistical limits by an additional 0.1 cm/sec to account for this error.

# APPENDICES

The first three appendices contain resumés of the theory of the various interactions with which this thesis is concerned. They are not meant to be complete derivations of the various results that are obtained, but are presented here in order to round out our theoretical treatment and to clarify our notational conventions where necessary. The last two contain the detailed derivation of several formulas used in the text.

## APPENDIX I

## THE CRYSTALLINE ELECTRICAL FIELD INTERACTION

In this section we are concerned with describing the interaction of the crystalline electrical field (CEF) with the 4f electrons of a rare earth ion. As mentioned before, the CEF interaction is weak compared to the spin orbit interaction so that the CEF interaction can be treated as perturbing a manifold of states for which J, the total angular momentum, is a good quantum number. We therefore, treat here only the interaction with a single J-multiplet and do not consider the mixing of states of different J. The potential energy of an electron located at the position $(r, \theta, \phi)$ due to the surrounding ions may be expanded in a series as

$$- e\, V(r,\theta,\phi) = \sum_{n} \sum_{m=-n}^{+n} A_n^m r^n \Phi_n^m(\theta,\phi) \qquad (41)$$

where $\Phi_n^m$ and $\Phi_n^{-m}$ are the real and imaginary parts of the spherical harmonics $Y_n^m$, but with different normalization. Specifically, we use the normalization[13]

$$\Phi_{2n}^0 = 2^n\, n!\, P_{2n}(\cos\theta)$$

$$\Phi_n^{\pm m} = 2^m\, m!\, \frac{(n-m)!}{(n+m)!}\, P_n^m(\cos\theta)\, x \begin{Bmatrix} \cos m\phi \\ \sin m\phi \end{Bmatrix} m > 0 \qquad (42)$$

with

$$P_n^m(x) = (1 - x^2)^{m/2} \left(\frac{d}{dx}\right)^m P_n(x)$$

where $P_n$ is a Legendre polynomial. In particular, for n = 2 we have

$$\Phi_2^{\,0} = 3\cos^2\theta - 1 = (3z^2 - r^2)/r^2$$

$$\Phi_2^{\,1} = \sin\theta\cos\theta\cos\phi = z\,x\,/r^2$$

$$\Phi_2^{-1} = \sin\theta\cos\theta\sin\phi = z\,y/r^2 \qquad (43)$$

$$\Phi_2^{\,2} = \sin^2\theta\cos 2\phi = (x^2 - y^2)/r^2$$

$$\Phi_2^{-2} = \sin^2\theta\sin 2\phi = 2\,x\,y/r^2.$$

The direct interaction with the 4f electrons is, in effect, partially shielded by the closed electron shell. That is, the CEF will distort the closed shells so that an additional potential is produced, which may be expanded as

$$-e\,V'(r,\theta,\phi) = \sum_{n,m} A_n^{\,m} S_n(r)\,\Phi_n^{\,m}(\theta,\phi). \qquad (44)$$

Consequently, the Hamiltonian for the 4f electrons is

$$H_{CEF}^{4f} = \sum_k \sum_{n,m} A_n^{\,m}\left[r_k^{\,n} + S_n(r_k)\right]\Phi_n^{\,m}(\theta_k,\phi_k). \qquad (45)$$

Since we are concerned only with a single J-multiplet we may use operator equivalents[14] to rewrite this Hamiltonian as

$$H_{CEF}^{4f} = \sum_{n,m} A_n^{\,m}\langle r^n\rangle_E \langle J||\theta_n||J\rangle\, O_n^{\,m}(\vec{J}) \qquad (46)$$

where

$$\langle r^n\rangle_E = (1 - \sigma_n)\langle r^n\rangle_{4f}$$

$$\sigma_n\langle r^n\rangle_{4f} = \langle S_n(r)\rangle_{4f},$$

the symbol $\langle r^n \rangle_{4f}$ denotes the matrix element of $r^n$ for the radial part of the 4f wavefunction. The expressions $\langle J||\theta_n||J\rangle$ are reduced matrix elements which have been tabulated in the literature[10]. The usual notation is $\theta_n = \alpha,\beta,\gamma$ for $n = 2,4,6$. The $O_n^m(\vec{J})$ are the operator equivalents - $n^{th}$ order polynomials in $J$, $J_z$, $J_+$, and $J_-$. The relevant operator equivalents are tabulated in reference 13. In particular for $n = 2$ they are

$$O_2^0 = 3J_z^2 - J^2$$

$$O_2^1 = 1/4\ J_z(J_+ + J_-) + (J_+ + J_-)J_z = 1/2(J_zJ_x + J_xJ_z)$$

$$O_2^{-1} = 1/4i\ J_z(J_+ - J_-) + (J_+ - J_-)J_z = 1/2(J_zJ_y + J_yJ_z) \qquad (47)$$

$$O_2^2 = 1/2\ (J_+^2 + J_-^2) = J_x^2 - J_y^2$$

$$O_2^{-2} = 1/2i(J_+^2 - J_-^2) = J_xJ_y + J_yJ_x\ .$$

For the case of a two-fold symmetry axis only $n = 2,4,6$ with even $m$ need be considered when the z axis is taken along the two-fold axis.

In principle, it is possible to calculate both $A_n^m$ and $\langle r^n \rangle$, but in practice it is difficult to do so. Consequently, the CEF parameters are introduced since it is these that are deduced from the optical spectra:

$$C_n^m = A_n^m \langle r^n \rangle. \qquad (48)$$

(These are also denoted $B_n^m$ in the literature.) The CEF parameters for $TmCl_3 \cdot 6H_2O$ were obtained by modifying Harrop's $ErCl_3 \cdot 6H_2O$ parameters[8], using the calculated $\langle r^n \rangle$ of Freeman and Watson[15] and

assuming the $A_n^m$ were unchanged. Using these CEF parameters the wavefunctions were calculated in the form

$$|i\rangle = \sum_{m=-6}^{6} a_m^i |m\rangle \tag{49}$$

where $|m\rangle$ are eigenstates of $J_z$. The coefficients $a_m^i$ are tabulated in Table II for the two lowest states $|G\rangle$ and $|E\rangle$. Also tabulated are the matrix elements of $\langle G|O_2^m|G\rangle$, $\langle E|O_2^m|E\rangle$, $\langle E|O_2^m|G\rangle$, and $\langle E|\vec{J}|G\rangle$, which are the ones relevant to the hyperfine interactions.

TABLE II

Wave Functions and Matrix Elements of the Two Lowest CEF Levels of $Tm\,Cl_3 \cdot 6H_2O$

The wavefunctions are written in the form $|i\rangle = \sum_m a_m^i |J,m\rangle$ with $J = 6$ and $a_{-m}^i = a_m^{i*}$. The coefficients $a_m^i$ are tabulated here for $m \geq 0$.

These wavefunctions were calculated from CEF parameters from Harrop[8]: $C_2^0 = 111$, $C_2^2 = 152$, $C_2^{-2} = -252$, $C_4^0 = -82$, $C_4^2 = -179$, $C_4^{-2} = 320$, $C_4^4 = 308$, $C_4^{-4} = 146$, $C_6^0 = -9$ $C_6^2 = -62$, $C_6^{-2} = 126$, $C_6^4 = 212$, $C_6^{-4} = -106$, $C_6^6 = 212$, $C_6^{-6} = -10$.

The reduced matrix elements used were: $\langle J||\alpha||J\rangle = 1.02 \times 10^{-2}$, $\langle J||\beta||J\rangle = 1.59 \times 10^{-4}$, $\langle J||\gamma||J\rangle = -5.53 \times 10^{-6}$. The two levels are separated in energy by $0.63\ cm^{-1}$.

| State | m | 0 | 1 | 2 | 3 | 4 | 5 | 6 |
|---|---|---|---|---|---|---|---|---|
| $\|G\rangle$ | $Re(a_m)$ | 0 | 0.373 | 0 | -0.222 | 0 | 0.081 | 0 |
| | $Im(a_m)$ | | -0.542 | | -0.098 | | 0.033 | |
| $\|E\rangle$ | $Re(a_m)$ | 0.722 | 0 | -0.133 | 0 | -0.065 | 0 | 0.059 |
| | $Im(a_m)$ | 0 | | 0.452 | | 0.078 | | -0.060 |

Table IIA Wavefunctions

| Matrix Element \ m | -2 | -1 | 0 | 1 | 2 |
|---|---|---|---|---|---|
| $\langle G\|O_2^m\|G\rangle$ | 28.9 | 0 | -35.0 | 0 | -9.9 |
| $\langle G\|O_2^m\|E\rangle$ | 0 | 0.23i | 0 | -0.22i | 0 |
| $\langle E\|O_2^m\|E\rangle$ | 29.4 | 0 | -35.2 | 0 | -9.9 |
| | | $J_y$ | $J_z$ | $J_x$ | |
| $\langle G\|\vec{J}\|E\rangle$ | | 4.78 | 0 | 3.46 | |

Table IIB Matrix Elements

## APPENDIX II

## THE NUCLEAR ELECTRIC QUADRUPOLE INTERACTION

The electric quadrupole interaction of the nucleus with the surrounding charges may be written[16]

$$H_Q = \frac{e^2 Q}{2I(2I - I)} \sum_{i,j} 1/2\ q_{ij}\ (I_i I_j + I_j I_j - 2/3\ \vec{I}^2 \delta_{ij}) \tag{50}$$

with i,j = x,y,z. Q is the nuclear quadrupole moment, $I_x$, $I_y$, $I_z$ are components of the nuclear spin operator, $\vec{I}$, and $\vec{I}^2 = I(I + 1)$. The tensor $q_{ij}$ is the field gradient tensor of the surrounding charges.

The diagonal terms of Eq. (50) may be written as

$$q_{xx}(I_x^2 - 1/3\ \vec{I}^2) + q_{yy}(I_y^2 - 1/3\ \vec{I}^2) + q_{zz}(I_z^2 - 1/3\ \vec{I}^2) \tag{51}$$

$$= 1/2\ q_{zz}(3I_z^2 - \vec{I}^2) + (q_{xx} - q_{yy})(I_x^2 - \vec{I}_y^2)$$

where we have used $\vec{I}^2 = I_x^2 + I_y^2 + I_z^2$, and Laplace's equation

$$q_{xx} + q_{yy} + q_{zz} = 0\ . \tag{52}$$

Since the tensor $\langle q_{ij} \rangle$ is symmetric, there will be a coordinate system in which it is diagonal. In this case we see from Eq. (51) that the field gradient can be characterized by two numbers, $\langle q_{zz} \rangle$ and $\eta = \langle q_{xx} - q_{yy} \rangle / \langle q_{zz} \rangle$, the latter being a measure of the departure from axial symmetry.

Combining the equations (47), (50) and (51) we may make use of the $O_n^m$ operators introduced in Appendix I

$$H_Q = \frac{e^2 Q}{4I(2I - 1)} \sum_i q^i \, O_2^i(\vec{I}) \tag{53}$$

where we define

$$\begin{aligned} q^0 &= q_{zz} \\ q^1 &= 2(q_{zx} + q_{xz}) = 4\, q_{xz} \\ q^{-1} &= 2(q_{zy} + q_{yz}) = 4\, q_{yz} \\ q^2 &= (q_{xx} - q_{yy}) \\ q^{-2} &= (q_{xy} + q_{yx}) = 2\, q_{xy}. \end{aligned} \tag{54}$$

The electric field gradient which interacts with a rare earth nucleus in an ionic crystal has four significant sources: (1) The field gradient produced at the nuclear site by the surrounding ions; (2) The field gradient produced at the nuclear site by the partially filled 4f shell of the ion containing the nucleus in question; (3) The "lattice" Sternheimer effect whereby source (1) introduces a distortion in the closed electron shells, producing a shielding of source (1); (4) The "atomic" Sternheimer effect, which shields the 4f contribution to the field gradient. Collecting the different contributions, we have for the total field gradient tensor

$$q_{ij} = (1 - \gamma_\infty)\, q_{ij}^{(lat)} + (1 - R_Q)\, q_{ij}^{(4f)} \tag{55}$$

where $\gamma_\infty$ and $R_Q$ are the lattice and atomic Sternheimer shielding factors, respectively. Source (1) is usually small compared to the

other sources; source (3) in rare earths is usually a large anti-shielding term, i.e., $\gamma_\infty$ is a large negative number ($\sim -10^2$) so that source (3) is comparable to (2) and (4).

For the contribution from the lattice (the surrounding ions) we can use the potential in Eq. (41). The quadrupole tensor is then given by

$$q_{ij} = [\partial^2 V(\vec{r})/\partial x_i \, \partial x_j]_{r=0} \tag{56}$$

hence, after a little algebra we find that

$$e^2 \, q^i_{(lat)} = -4 \, A_2{}^i \tag{57}$$

where the $q^i$ were defined in Eq. (54).

For the 4f electrons we may use the method of operator equivalents[14] to obtain

$$q_{ij}^{(4f)} = -3\langle J||\alpha||J\rangle\langle r^{-3}\rangle_{4f}[1/2\ (J_iJ_j + J_jJ_i) - 1/3\ J^2\delta_{ij}] \tag{58}$$

combining these contributions, we obtain after a little more algebra

$$\begin{aligned}
q^0 &= -P\, O_2{}^0(\vec{J}) - 4(1-\gamma_\infty)A_2{}^0/e^2 \\
q^1 &= -12\, P\, O_2{}^1(\vec{J}) - 4(1-\gamma_\infty)A_2{}^1/e^2 \\
q^{-1} &= -12\, P\, O_2^{-1}(\vec{J}) - 4(I-\gamma_\infty)A_2^{-1}/e^2 \\
q^2 &= -3\, P\, O_2{}^2(\vec{J}) - 4(1-\gamma_\infty)A_2{}^2/e^2 \\
q^{-2} &= -3\, P\, O_2^{-2}(\vec{J}) - 4(1-\gamma_\infty)A_2^{-2}/e^2
\end{aligned} \tag{59}$$

where $P = \langle J||\alpha||J\rangle \langle r^{-3}\rangle_Q$, and

$$\langle r^{-3}\rangle_Q = (1 - R_Q)\langle r^{-3}\rangle_{4f}. \qquad (60)$$

For $TmCl_3 \cdot 6H_2O$ only a few of these operators have non-zero matrix elements. Due to the two-fold symmetry the matrix elements $\langle\rho|O_n^m|\rho\rangle = 0$ for odd m, where $|\rho\rangle$ is a CEF state. On the other hand $\langle E|O_n^m|G\rangle = 0$ for even m while $\langle E|O_2^{\pm 1}|G\rangle$ are both quite small. The latter matrix elements will produce a slight shift of the center of gravity at low temperatures, but this is negligible compared to the magnetic interaction (see next section). So, for our purposes that leaves us with only $q^0$, $q^2$, and $q^{-2}$. In the principal axis coordinate system of the tensor $\langle q_{ij}\rangle$, $\langle q^{-2}\rangle$ is zero by definition; this does not imply, however, that the principal axes will be the same for each of the CEF levels. To put this another way, we may choose our coordinate system to be the one for which $A_2^{-2} = 0$, say, then it will <u>not</u> be true in general that $\langle\rho|O_2^{-2}|\rho\rangle = 0$ when the lattice has only two-fold symmetry[17]. As can be seen from Table II the field gradients from the two lowest CEF states of $TmCl_3 \cdot 6H_2O$ are nearly identical. The coordinate systems for which $\langle O_2^{-2}(\vec{J})\rangle$ vanishes are nearly coincident, they are rotated with respect to each other by only $\sim 0.2^\circ$, while the coordinate system for which $A_2^{-2} = 0$ differs by $\sim 6^\circ$.

## APPENDIX III

### THE NUCLEAR MAGNETIC DIPOLE INTERACTION

The magnetic hyperfine interaction between the nucleus and the surrounding 4f shell is[18]

$$H_M = 2\beta g \beta_N \sum_i [\vec{\ell}_i / r_i^3 - \vec{s}_i / r_i^3 + 3\vec{r}_i (\vec{s}_i \cdot \vec{r}_i)/r_i^5] \cdot \vec{I} \quad (61)$$

where $\beta$ is the Bohr magneton, g the nuclear g factor, I the nuclear spin, $r_i$ the radius vector of the $i^{th}$ electron, and $\ell$ and s the orbital and spin angular momenta, and where we have left out the so-called Fermi contact term, which is negligible for the 4f electrons. Again, using operator equivalents we may also write[10,14]

$$H_M = g\beta_N M \vec{J} \cdot \vec{I} \quad (62)$$

where $M = 2\beta \langle J||N||J\rangle \langle r^{-3}\rangle_M$ and $\langle r^{-3}\rangle_M$ is defined analogously to $\langle r^{-3}\rangle_Q$, $\langle r^{-3}\rangle_M = (1 - R_M)\langle r^{-3}\rangle_{4f}$ (Eq. (46)).

The only non-zero matrix elements of $\vec{J}$ in $TmCl_3 \cdot 6H_2O$ are between CEF states, e.g., $\langle E|\vec{J}|G\rangle$. Due to symmetry under time-reversal, the diagonal matrix elements of $\vec{J}$, e.g. $\langle G|\vec{J}|G\rangle$, must vanish for non-degenerate states in the absence of an external magnetic interaction. In this case "external" means anything outside the ion in question, including magnetic interactions with surrounding ions; these are excluded, by definition, in the CEF theory. As it happens the direction of $\langle E|\vec{J}|G\rangle$ lies parallel, within about $1^o$, to a principle axis of the field gradient tensor.

## APPENDIX IV

## CENTER OF GRAVITY SHIFT DUE TO THE MAGNETIC HYPERFINE INTERACTION

In this section we will derive a general formula for the shift of the center of gravity of the Mössbauer spectrum due to a magnetic hyperfine interaction between two nearly degenerate 4f levels. To do this, we will use second order perturbation theory, so that we will need to assume that the magnetic hyperfine interaction is smaller than the CEF splitting, $k\theta$, of the nearly degenerate 4f levels.

For the states of the combined nuclear-electronic system we write

$$|G,k\rangle = \sum_m a_m^k |G\rangle|I,m_I\rangle$$
$$|E,\ell\rangle = \sum_m b_m^\ell |E\rangle|I,m_I\rangle \qquad (63)$$

where $|G,k\rangle$ and $|E,\ell\rangle$ are the eigenstates of the quadrupole hyperfine interaction (not including terms like $\langle E|O_2^m(\vec{J})|G\rangle$- see Appendix III). We will neglect the quadrupole hyperfine energies in the energy denominators since they constitute a third order term. The second order shift of the energy of the $k^{th}$ level of the ground state is given by

$$E_G^k = \frac{-1}{k\theta} \sum_{\ell} |\langle E,\ell | g\, \beta_N\, M\, \vec{I} \cdot \vec{J}\, | G,k\rangle|^2$$

$$= \frac{-1}{k\theta} \sum_{\ell} \Big| \sum_{m,m'} a_m^k\, b_{m'}^{\ell *} g\beta_N M \langle E|\vec{J}|G\rangle \cdot \langle m'|\vec{I}|m\rangle \Big|^2 \qquad (64)$$

$$= \frac{-g^2\beta_N^2 M^2}{k\theta} \sum_{\ell} \sum_{\substack{m_1,m_2 \\ m_3,m_4}} a_m^k,\ a_{m_2}^{k*}\, b_{m_3}^{\ell}\, b_{m_4}^{\ell *}\, (\vec{K} \cdot \langle m_4|\vec{I}|m_1\rangle)(\langle m_2|\vec{I}|m_3\rangle \cdot \vec{K}^*)$$

where we write $\vec{K} = \langle E|\vec{J}|G\rangle$.

The average shift of the levels associated with the ground electronic state is

$$-E_{shift} = \frac{1}{2I+1} \sum_k E_G^k \ . \qquad (65)$$

Using closure:

$$\sum_k a_{m_1}^k\, a_{m_2}^{k*} = \delta_{m_1 m_2}$$

$$\sum_{\ell} b_{m_3}^{\ell}\, b_{m_4}^{\ell *} = \delta_{m_3 m_4} \ . \qquad (66)$$

We get from (64) and (65)

$$E_{shift} = \frac{g^2\beta_N^2 M^2}{k\theta(2I+1)} \sum_{m,m'} (\langle m|\vec{I}|m'\rangle \cdot \vec{K})(\langle m'|\vec{I}|m\rangle \cdot \vec{K}^*) . \qquad (67)$$

At this point we might note that neglecting the quadrupole hyperfine energies in the denominators amounts to assuming that all the $|G,k\rangle$ are degenerate. Hence, we could have just as well chosen our states to be $|G\rangle|I,m\rangle$ and written down (67) almost immediately. Proceeding,

we may write $\vec{I} \cdot \vec{J} = I_z J_z + 1/2(I_+ J_- + I_- J_+)$, then (67) becomes

$$E_{shift} = \frac{g^2 \beta_N{}^2 M^2}{k\theta(2I+1)} \left[ |J_z|^2 \sum_m |\langle m|I_z|m\rangle|^2 + \frac{1}{4}(|J_+|^2 + |J_-|^2) \sum_m |\langle m|I_+|m-1\rangle|^2 \right] \tag{68}$$

where $|J_z|^2 = |\langle G|J_z|E\rangle|^2$ etc.

It is easy to show that

$$\sum_m |\langle m|I_z|m\rangle|^2 = 1/3\ I(I+1)\ (2I+1)$$
$$\sum_m |\langle m|I_+|m-1|^2 = 2/3\ I(I+1)(2I+1) \tag{69}$$

and

$$|J_+|^2 + |J_-|^2 = 2(|J_x|^2 + |J_y|^2)\ . \tag{70}$$

Gathering everything together we get

$$E_{shift} = 1/3\ \frac{g^2 \beta_N{}^2 M^2}{k\theta} I(I+1) |\langle G|\vec{J}|E\rangle|^2 . \tag{71}$$

For $Tm\ Cl_3 \cdot 6H_2O$ it happens that the third order term of the perturbation expansion is nearly zero. The magnetic interaction has only even order terms since odd order terms all involve matrix elements of $\langle G|\vec{J}|E\rangle$ or $\langle E|\vec{J}|E\rangle$ which are zero. Consequently, the only third order term comes from neglecting the quadrupole energies in the energy denominator.

Assuming that the field gradients are axially symmetric and $\langle G|\vec{J}|E\rangle$ lies parallel to this symmetry axis, the unperturbed states are

$$|G\rangle|I,m_I\rangle \qquad E = E_m$$
$$|E\rangle|I,m_I\rangle \qquad E = k\theta + E'_m \tag{72}$$

for $I = 3/2, E_{\pm 3/2} = -E_{\pm 1/2}$ the third order term is then

$$E^{(3)} = \frac{g^2\beta_N{}^2M^2}{k^2\theta^2(2I+1)} J_z{}^2 \sum_m m_1{}^2(E'_m - E_m)$$
$$E^{(3)} = \frac{4g^2\beta_N{}^2M^2}{k\theta(2I+1)} J_z{}^2 \left[(E_{3/2} - E'_{3/2})/k\theta\right] . \tag{73}$$

For $Tm\,Cl_3 \cdot 6H_2O$ the field gradients of the two nearly degenerate CEF levels are almost the same. Consequently $E'_{3/2} \sim E_{3/2}$ and $E^{(3)} \sim 0$.

## APPENDIX V

## SHAPE OF MÖSSBAUER SPECTRAL LINES INFLUENCED BY ELECTRONIC RELAXATION

In this section we derive the shape of Mössbauer spectral lines influenced by relaxation between the electronic states. In the limit of very long relaxation times we would expect to see a superposition of the hyperfine spectra of each of the electronic states, weighted with the appropriate Boltzman factors. On the other hand if the relaxation times are very short, we would expect to see a hyperfine spectrum appropriate to the thermally averaged electric and magnetic fields. Here we will be interested in the intermediate region where the relaxation times are neither particularly fast nor particularly slow. This treatment uses Anderson's "random frequency-modulation model" [9] as a basis. The relevant sections of his paper are sections 1 and 2 and section 4 up to equation (50) near the bottom of page 326 (there is another equation labeled (50) on the preceding page). Since this is a fairly lengthy derivation we will not repeat it all here. We will, however, indicate several minor adaptations needed for our problem.

For our case, the parts of the Hamiltonian are:
$H_0$ includes the interactions of the free ion except for the hyperfine interactions. $H_p$ includes the hyperfine interactions and the static CEF interactions. $H_m$ includes the interaction which causes relaxation between the CEF levels.

We wish to include explicitly the fact that our spectrum

lines have a finite width in the absence of relaxation. This can be done by making the spectral frequencies complex: we replace $\Delta\omega_{ij}$ by $\Delta\omega_{ij} + i\Gamma$. This has the effect of adding $-\Gamma$ to all the diagonal elements of the matrix $\underline{i\Delta\omega + \Pi}$. This has no effect on the matrix eigenvectors, which are the columns of the transformation matrix $\underline{T}$. It does, however, have the effect of adding $-\Gamma$ to all the eigenvalues of the matrix. Consequently the autocorrelation function $\varphi(\tau)$ in Anderson's paper is multiplied by $e^{-\Gamma\tau}$, or equivalently, our spectrum will be obtained from Anderson's $I(\omega)$ by convolution with a Lorentzian of width (FWHM) $2\Gamma$.

Anderson implicitly assumes in his derivation that $\tau$ is positive. It is quite straightforward to show from the definition of $\varphi(\tau)$,

$$\varphi(\tau) = \int_{-\infty}^{\infty} \mu(t)\mu^*(t+\tau)dt \tag{74}$$

that

$$\varphi(-\tau) = \varphi^*(\tau) \tag{75}$$

we then get for the spectrum

$$\begin{aligned} I(\omega) &= \int_{-\infty}^{\infty} \varphi(\tau) e^{-i\omega\tau} d\tau \\ &= \int_{0}^{\infty} \varphi(\tau) e^{-i\omega\tau} d\tau + \int_{0}^{\infty} \varphi^*(\tau) e^{i\omega\tau} d\tau \\ &= 2\ \mathrm{Re}\left( \int_{0}^{\infty} \varphi(\tau) e^{-i\omega\tau} d\tau \right) \end{aligned} \tag{76}$$

where Re(x) means the real part of x.

From Anderson's equation (50) on page 326 we have that

$$\varphi(\tau) = \sum_k \left( \sum_i W_{1_i} T_{ik} \right) \left( \sum_j (T^{-1})_{kj} \right) e^{(\lambda_k - \Gamma)\tau} \tag{77}$$

and hence

$$I(\omega) = 2 \text{ Re } \left( \sum_k \frac{C_k}{i\omega + \Gamma - \lambda_k} \right) \tag{78}$$

where

$$C_k = \left( \sum_i W_{1_i} T_{ik} \right) \left( \sum_j (T^{-1})_{kj} \right) \tag{79}$$

so that we have finally

$$I(\omega) = 2 \sum_k \frac{\text{Im}(C_k)[\omega - \text{Im}(\lambda_k)] + \text{Re}(C_k)[\Gamma - \text{Re}(\lambda_k)]}{[\omega - \text{Im}(\lambda_k)]^2 + [\Gamma - \text{Re}(\lambda_k)]^2} , \tag{80}$$

Im(x) denotes the imaginary part of x.

The case we are interested in can be described in the following fashion: we have two hyperfine spectrum lines separated in the spectrum by $2\omega_0$; for convenience we will take $\omega = 0$ to be halfway in between these lines. We will denote the transition probabilities by $\omega_a$ and $\omega_b$ where $\omega_a$ is defined by assuming that at $t = 0$ the electrons are in the state associated with the line at $-\omega_0$, then $\omega_a$ is the probability that at $t = dt$ they are in the state associated with the line at $\omega_0$, $\omega_b$ is similarly defined for the reverse transition. For convenience we will also define

$$\begin{aligned} \omega_e &= 1/2 \quad (\omega_a + \omega_b) \\ \delta &= (\omega_b - \omega_a)/(\omega_b + \omega_a) \\ x &= \omega_0/\omega_e . \end{aligned} \tag{81}$$

We then have the following matrices:

$$\underline{\underline{\Delta\omega}} = \begin{bmatrix} -\omega_0 & 0 \\ 0 & \omega_0 \end{bmatrix}$$

$$\underline{\underline{\Pi}} = \begin{bmatrix} -\omega_a & \omega_a \\ \omega_b & -\omega_b \end{bmatrix} \qquad (82)$$

$$\underline{W_1} = \frac{1}{2}\begin{bmatrix} 1 + \delta \\ 1 - \delta \end{bmatrix}$$

$W_{1_i}$ is the (steady state) probability that state i is occupied. The eigenvalues of $\underline{\underline{(i\Delta\omega + \Pi)}}$ are the solutions of

$$(\lambda + \omega_a + i\omega_0)(\lambda + \omega_b - i\omega_0) - \omega_a\omega_b = 0$$

$$\lambda_1 = -\omega_e + (\omega_e^2 - \omega_0^2 - 2i\omega_e\omega_0\delta)^{1/2} \qquad (83)$$

$$\lambda_2 = -\omega_e - (\omega_e^2 - \omega_0^2 - 2i\omega_e\omega_0\delta)^{1/2}.$$

The un-normalized eigenvectors are:

$$\begin{bmatrix} \omega_a \\ \Omega \end{bmatrix} \quad \text{and} \quad \begin{bmatrix} \Omega \\ -\omega_b \end{bmatrix} \qquad (84)$$

where $\Omega = i\omega_0 - \omega_e\delta + (\omega_e^2 - \omega_0^2 - 2i\omega_e\omega_0\delta)^{1/2}$. One possible transformation matrix is

$$\underline{T} = \begin{bmatrix} \omega_a & \Omega \\ \Omega & -\omega_b \end{bmatrix} \qquad (85a)$$

and

$$\underline{\underline{T}}^{-1} = N^{-1}\begin{bmatrix} \omega_b & \Omega \\ \Omega & -\omega_a \end{bmatrix} \tag{85b}$$

with $N = \omega_a\omega_b + \Omega^2 = 2(\omega_e^2 - \omega_0^2 - 2i\omega_e\omega_0\delta)^{1/2}\Omega$. After some algebra we find that

$$\begin{aligned} C_1 &= 1/2[1 + (1 - ix\delta)(1 - 2ix\delta - x^2)^{1/2}] \\ C_2 &= 1/2[1 - (1 - ix\delta)(1 - 2ix\delta - x^2)^{1/2}] \ . \end{aligned} \tag{86}$$

In particular, we note that Im $(C_1)$ = - Im$(C_2)$. This is particularly important as it ensures that $I(\omega)$ drops off as $1/\omega^2$ for large $\omega$. Using Eq. (78) we write

$$I(\omega) = \frac{-iC_1}{\omega - i\Gamma + i\lambda_1} + \frac{iC_1^*}{\omega + i\Gamma - i\lambda_1^*} + \frac{-iC_2}{\omega - i\Gamma + i\lambda_2} + \frac{iC_2^*}{\omega + i\Gamma - i\lambda_2^*} \ . \tag{87}$$

This form is particulary useful for finding the center of gravity of the spectrum, $\bar{\omega}$, by the method of residues.

$$\bar{\omega} = \frac{\int_{-\infty}^{\infty} \omega I(\omega)\, d\omega}{\int_{-\infty}^{\infty} I(\omega)\, d\omega} \ . \tag{88}$$

Strictly speaking the integral in the numerator diverges logarithmically if the limits to infinity are taken separately. Consequently, a certain amount of sophistication must be used in the handling of the residues. Evaluating the integrals, we find that

$$\int_{-\infty}^{\infty} I(\omega)\, d\omega = 2\pi(C_1 + C_2) = 2\pi \tag{89}$$

$$\int_{-\infty}^{\infty} \omega\, I(\omega)\, d\omega = 2\pi\, \mathrm{Im}[\, C_1(\lambda_1 - \Gamma) + C_2(\lambda_2 - \Gamma)\,] = -\,2\pi\, \omega_0 \delta \tag{90}$$

hence

$$\bar{\omega} = -\,\omega_0 \delta \tag{91}$$

which is just the weighted average of the two spectrum line positions $(+\omega_0,\ -\omega_0)$.

We will be particularly interested in the case where $\omega_e \gg \omega_0$ (fast relaxation) or $x \ll 1$ in which case we get

$$\begin{aligned} \lambda_1 &= \omega_e\, [-1 + (1 - 2ix\delta - x^2)^{1/2}] \\ \lambda_1 &\approx \omega_e\, [-ix\delta + 1/2\ x^2(\delta^2 - 1)] \\ \mathrm{Re}(\lambda_1) &\approx -(\omega_0^{\,2}/2\omega_e)(1 - \delta^2) \\ \mathrm{Im}(\lambda_1) &\approx -\omega_0 \delta \end{aligned} \tag{92}$$

$$\begin{aligned} \lambda_2 &= \omega_e\, [-1 - (1 - 2ix\delta - x^2)^{1/2}] \\ \lambda_2 &\approx \omega_e\, [-2 + ix\delta] \\ \mathrm{Re}(\lambda_2) &\approx -2\omega_e \\ \mathrm{Im}(\lambda_2) &= -\,\mathrm{Im}(\lambda_1) \approx \omega_0 \delta \end{aligned} \tag{93}$$

$$C_1 = 1/2\,[1 + (1 - ix\delta)(1 - 2ix\delta - x^2)^{1/2}]$$

$$C_1 \approx 1 + 1/2\, x^2(1 - 1/2\, \delta^2) + 1/4\, ix^3\delta(3 - 5\delta^2)$$

$$\mathrm{Re}(C_1) \approx 1 \qquad (94)$$

$$\mathrm{Im}(C_1) \approx 1/4\, x^3\delta(3 - 5\, \delta^2)$$

$$C_2 = 1/2\,[1 - (1 - ix\delta)(1 - 2ix\delta - x^2)^{1/2}]$$

$$C_2 \approx - 1/2\, x^2(1 - 1/2\, \delta^2) - 1/4\, ix^3\delta(3 - 5\delta^2)$$

$$\mathrm{Re}(C_2) \approx - 1/2\, x^2(1 - 1/2\, \delta^2) \qquad (95)$$

$$\mathrm{Im}(C_2) \approx - 1/4\, x^3\delta(3 - 5\, \delta^2).$$

We can regroup the terms in Eq. (72) to get

$$I(\omega) = \left[\frac{\mathrm{Re}(C_1)(\Gamma - \mathrm{Re}(\lambda_1))}{(\omega - \mathrm{Im}(\lambda_1))^2 + (\Gamma - \mathrm{Re}(\lambda_1))^2}\right] + \left[\frac{\mathrm{Im}(C_1)(\omega - \mathrm{Im}(\lambda_1))}{(\omega - \mathrm{Im}(\lambda_1))^2 + (\Gamma - \mathrm{Re}(\lambda_1))^2}\right.$$

$$\left. + \frac{\mathrm{Im}(C_2)(\omega - \mathrm{Im}(\lambda_2)) + \mathrm{Re}(C_2)(\Gamma - \mathrm{Re}(\lambda_2))}{(\omega - \mathrm{Im}(\lambda_1))^2 + (\Gamma - \mathrm{Re}(\lambda_2))^2}\right]. \qquad (96)$$

The term in the first bracket is simply a Lorentzian with area $\sim 2\pi$, height $\sim 1/(\Gamma - \mathrm{Re}(\lambda_1))$ and width $\Gamma - \mathrm{Re}(\lambda_1) = \Gamma + 1/2\ (\omega_0^2/\omega_e)(1 - \delta^2)$. For our case $\Gamma$ and $\omega_0$ are of the same order of magnitude ($\omega_0$ may be slightly larger), so that we may write $\Gamma \sim \omega_0 = x\,\omega_e$. Hence, the height is $\sim 1/x\omega_e$. On the other hand the largest that any of the other terms in the second bracket becomes in the region $\omega \sim \pm\,\omega_0$ is

of the order of $x^2/\omega_e$. Consequently the terms in the second bracket are of the order of $x^3$ smaller than the first term.

REFERENCES

1. A.C. Melissinos and S.P. Davis, Phys. Rev. 115, 130 (1959).

2. R.V. Pound and G.A. Rebka, Jr., Phys. Rev. Letters 4, 274 (1960).

3. S.V. Karyagin, Doklady Akademii Nauk SSSR 148, 1102 (1963) (Doklady Phys. Chem. 148. 110 (1963)).

4. A preliminary report of this section of the thesis was presented at the Los Angeles A.P.S. Meeting, Dec. 1965.
M.J. Clauser, E. Kankeleit, and R.L. Mössbauer, Bull. Am. Phys. Soc. 10, 1202 (1965).

5. S. Hüfner, private communication.

6. M. Marezio, H.A. Plettinger, and W.H. Zachariasen, Acta Cryst. 14, 234 (1961).

7. N.K. Bel'skii and Yu.T. Struchkov, Kristallogradiya 10, 21 (1965) (Soviet Physics - Crystallography 10, 15 (1965)).

8. I.H. Harrop, J. Chem. Phys. 42, 4000 (1965).

9. P.W. Anderson, J. Phys. Soc. Japan 9, 316 (1954).

10. R.J. Elliot and K.W.H. Stevens, Proc. Roy. Soc.(London), A218, 553 (1953).

10a. L.B. Asprey and F.H. Kruse, J. Inorg. Nucl. Chem. 13, 32 (1960).

11. F.T. Snively, Ph.D. thesis, Department of Physics, California Institute of Technology, Pasadena, 1965; see also reference 13 below and E. Kankeleit, Rev. Sci. Instr. 35, 194 (1964).

12. M. Kalvius, P. Kienle, H. Eicher, W. Wiedemann, and C. Schüler, Z. Physik 172, 231 (1963).

13. R.G. Barnes, R.L. Mössbauer, E. Kankeleit and J.M. Poindexter, Phys. Rev. 136, A175 (1964).

14. K.W.H. Stevens, Proc. Phys. Soc. (London) 65A, 209 (1952).

15. A.J. Freeman and R.E. Watson, Phys. Rev. 127, 2058 (1962).

16. H. Eicher, Z. Physik 169, 178 (1962).

17. Reference 13 mistakenly assumed that the matrix elements of $O_2^{-2}$ would be zero for $Tm_2O_3$.

18. A. Abragam and M.H.L. Pryce, Proc. Roy. Soc. (London) A205, 135 (1951).